

Nanostructured p-Type Semiconducting Transparent Oxides: Promising Materials for Nano-Active Devices and the Emerging Field of “Transparent Nanoelectronics”

Arghya Banerjee^{*1} and Kalyan K. Chattopadhyay²

¹Nevada Nanotechnology Center, Department of Electrical Engineering and Computer Science, University of Nevada, Las Vegas, Nevada-89154, USA, ²Thin Film and Nanoscience Laboratory, Department of Physics, Jadavpur University, Kolkata-700032, India

Received: December 26, 2007; Accepted: January 9, 2008; Revised: January 9, 2008

Abstract: Transparent conducting oxides (TCO) with p-type semiconductivity have recently gained renewed interest for the fabrication of all-oxide transparent junctions, having potential applications in the emerging field of ‘Transparent’ or ‘Invisible Electronics’. This kind of transparent junctions can be used as a “functional” window, which will transmit visible portion of solar radiation, but generates electricity by the absorption of the UV part. Therefore, these devices can be used as UV shield as well as UV cells. In this report, a brief review on the research activities on various p-TCO materials is furnished along-with the fabrication of different transparent p-n homojunction, heterojunction and field-effect transistors. Also the reason behind the difficulties in obtaining p-TCO materials and possible solutions are discussed in details. Considerable attention is given in describing the various patent generations on the field of p-TCO materials as well as transparent p-n junction diodes and light emitting devices. Also, most importantly, a detailed review and patenting activities on the nanocrystalline p-TCO materials and transparent nano-active device fabrication are furnished with considerable attention. And finally, a systematic description on the fabrication and characterization of nanocrystalline, p-type transparent conducting CuAlO₂ thin film, deposited by cost-effective low-temperature DC sputtering technique, by our group, is furnished in details. These p-TCO micro/nano-materials have wide range of applications in the field of optoelectronics, nanoelectronics, space sciences, field-emission displays, thermoelectric converters and sensing devices.

Keywords: P-type transparent conducting oxide (p-TCO), nanocrystalline p-TCO, transparent p-n junction, transparent field effect transistor (TFET), nano-active device, transparent nanoelectronics, delafossite structure, nonstoichiometry, p-type doping, p-CuAlO₂ nanoparticles, direct current (DC) sputtering, low-temperature deposition, quantum confinement effect, photoluminescence, p-type ZnO.

1. INTRODUCTION

1.1. P-type Transparent Conducting Oxide

Amongst various oxide materials, the most important oxide based materials that create overwhelming interest within materials scientists is the fundamental aspects and applications of semiconducting transparent films: more popularly known as “Transparent Conducting Oxides” (TCO), which are widely used for a long time in optoelectronics industries as well as in research fields [1-61]. The characteristics of such films are high room-temperature electrical conductivity ($\sim 10^3$ S cm⁻¹ or more) and high optical transparency (more than 80 %) in the visible region. The electronic band gap of a TCO is higher than 3.1 eV (corresponding to the energy of a 400 nm blue photon). So visible photons (having energy between 2.1 to 3.1 eV) cannot excite electrons from valence band (VB) to the conduction band (CB) and hence are transmitted through it, whereas they have enough energy to excite electrons from donor level to CB (for n-type TCO) or holes from acceptor level to VB (for p-type TCO). And these acceptor or donor levels are created in the TCOs by introducing non-stoichiometry and (or) appropriate dopants in a controlled manner. A schematic representation of the bandgap designing for transparent conductors is shown in Fig. (1).

metry and (or) appropriate dopants in a controlled manner. A schematic representation of the bandgap designing for transparent conductors is shown in Fig. (1).

Although the TCOs have vast range of applications, very little work has been done on the active device fabrication using TCOs [62, 63]. This is because most of the well-known and widely used TCOs are n-type semiconductors (n-TCO), whereas their p-type counterpart (p-TCO), which are essential for junctional devices, were surprisingly missing in thin film form for a long time. Only in the last decade Sato *et al.* [64] and Kawazoe *et al.* [65] reported the p-type conductivity in a transparent thin film of binary nickel oxide (p-Ni_{1-x}O) and delafossite copper aluminum oxide (p-CuAlO_{2+x}) [64] respectively. Thereafter, syntheses of a large number of p-TCO thin films with wide range of electro-optical properties have been reported in the last few years. Amongst this new group of TCOs, the most important is the delafossite structured p-TCO thin films in the form of A^IB^{III}O_{2+x} (A^I: Cu⁺, Ag⁺, B^{III}: Trivalent cations) and their doped versions [66-75]. Besides delafossite p-TCO thin films, some important non-delafossite p-TCO thin films have also been reported having very good electro-optical properties. These films include Cu₂Sc₂O₄ [76], spinel oxide films of the form A^{II}B^{III}₂O₄ (A^{II}: Ni²⁺, B^{III}: Co³⁺) [77-78], layered oxychalcogenide films of the form (Ln^{III}O)M^IC^h (Ln^{III}: La⁺³, Pr⁺³, Nd⁺³, Sm⁺³, Gd⁺³, Y⁺³, M^I: Cu⁺, Ag⁺, C^h: S²⁻, Se²⁻) [79-89], mixed oxide films of the form In₂O₃-Ag₂O

*Address correspondence to this author at the Nevada Nanotechnology Center, Department of Electrical Engineering and Computer Science, University of Nevada, Las Vegas, Nevada-89154, USA; Tel: +1 702 895 3777; Fax: +1 702 895 4075; E-mail: banerjee_arghya@hotmail.com

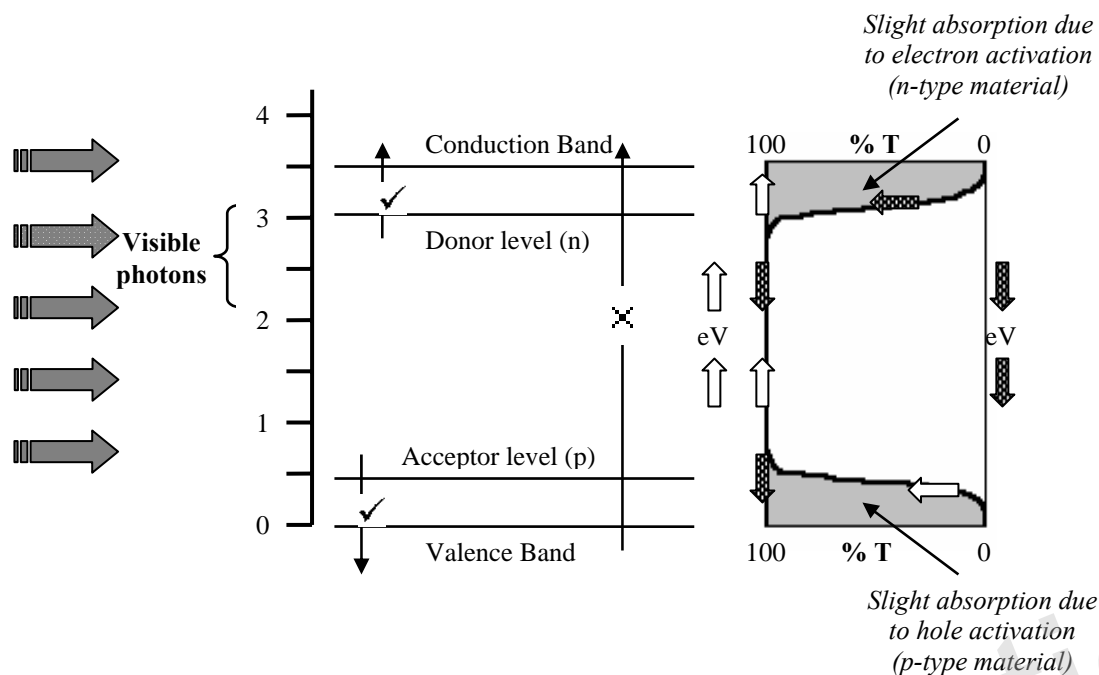


Fig. (1). Bandgap designing for transparent conductors. Visible photons (2.1 eV to 3.1 eV) do not have enough energy to excite electrons from valence band to conduction band, but have enough energy to excite holes (for p-type) from acceptor level to VB or electrons (for n-type) from donor level to CB. Right hand side shows the transmittance graph for a p-type TCO, where a slight absorption can be observed (indicated by shaded part) at low energy region, due to the activation of holes from acceptor level to VB. Similarly, the arrow '→' indicates the same for n-type TCO, where slight absorption at low energy region takes place due to electron activation from donor level to CB.

[90], binary oxide films like Ni_{1-x}O [64] and p-ZnO etc. [91-101]. A chart of various groups of p-TCO thin films, reported so far, has been shown in Fig. (2). Also the electrical and optical properties of various delafossite and non-delafossite p-TCO thin films are furnished in Table 1 and Table 2 respectively. The deposition techniques involved in the syntheses of these p-TCO thin films include pulsed laser deposition (PLD) [66-67, 76, 101-105], sputtering [64, 69-71, 74, 78-81, 84, 90, 104, 106-117], chemical vapor deposition (CVD) [96, 118-120], Reactive Solid Phase Epitaxy [121-123], Molecular beam epitaxy [98], Thermal co-evaporation [69, 72], Electron-beam evaporation [124-125], Rapid thermal annealing [126], sol-gel synthesis [110-111, 127, 128], hydrothermal process [69, 129-130], spray pyrolyses [131], spin coating [77] etc. Deposition parameters of different p-TCO thin films grown by various techniques are tabulated in Table 3 to Table 7. It is noteworthy in this context that there are reports on the fabrication of non-oxide p-type transparent semiconductors like BaCu_2S_2 , BaCuSF [132-134] etc. Although these materials cannot be classified as p-TCO, but still they have scientific importance in the field of transparent active device fabrication.

1.2. Transparent Electronics

The importance of this new group of p-TCOs lies in the fact that the transparent junction with both types of TCOs can be fabricated as a 'functional' window, which would absorb the UV part of the solar radiation to generate electricity, yet transmits the visible portion of it. This has opened up a new field in opto-electronics device technology, which is called "Transparent Electronics" or "Invisible

Electronics" [53, 135]. The first report of a semi-transparent all-oxide p-i-n heterojunction diode of the form p-NiO/i-NiO/i-ZnO/n-ZnO was published in 1993 by Sato co-authors [64] in 1993. They observed only 20 % transmittance of the diode in the visible region. Although this low transmittance was not favorable for superior device applications, but still this report was an important milestone in the field of "Transparent Electronics" and in the development of p-TCO technology. Thereafter, a large number of groups reported the fabrication of all-TCO p-n and p-i-n heterojunction [72, 136-145] and homojunction [68, 146-148] transparent diodes as well as transparent field effect transistors (TFET) [53, 149-155] on glass and various transparent substrates. A schematic diagram of an all-TCO diode and a TFET are shown in Fig. (3a) and Fig. (3b) respectively. For all-TCO diodes, the visible transparency of the device varies from less than 20 % to more than 80 % whereas the turn-on voltage ranges from 2.5 to 0.4 V. For heterojunctions, the efficiency of the diode deteriorates due to lattice mismatch whereas homojunction diodes are favored as the lattice matching seems to be natural, which improves the diode efficiency. In TFETs, the maximum transparency of the device had been reported to be 80 % with on-off ratio ranging from 10^4 to 10^7 . Various parameters of different all-transparent diodes are furnished in Table 8 whereas deposition routes and various parameters of different TFETs are furnished in Table 9.

1.3. Nanocrystalline p-TCO

After the pioneering works of Efros and Efros [156] and Brus [157] on the size-quantization effect in semiconductor

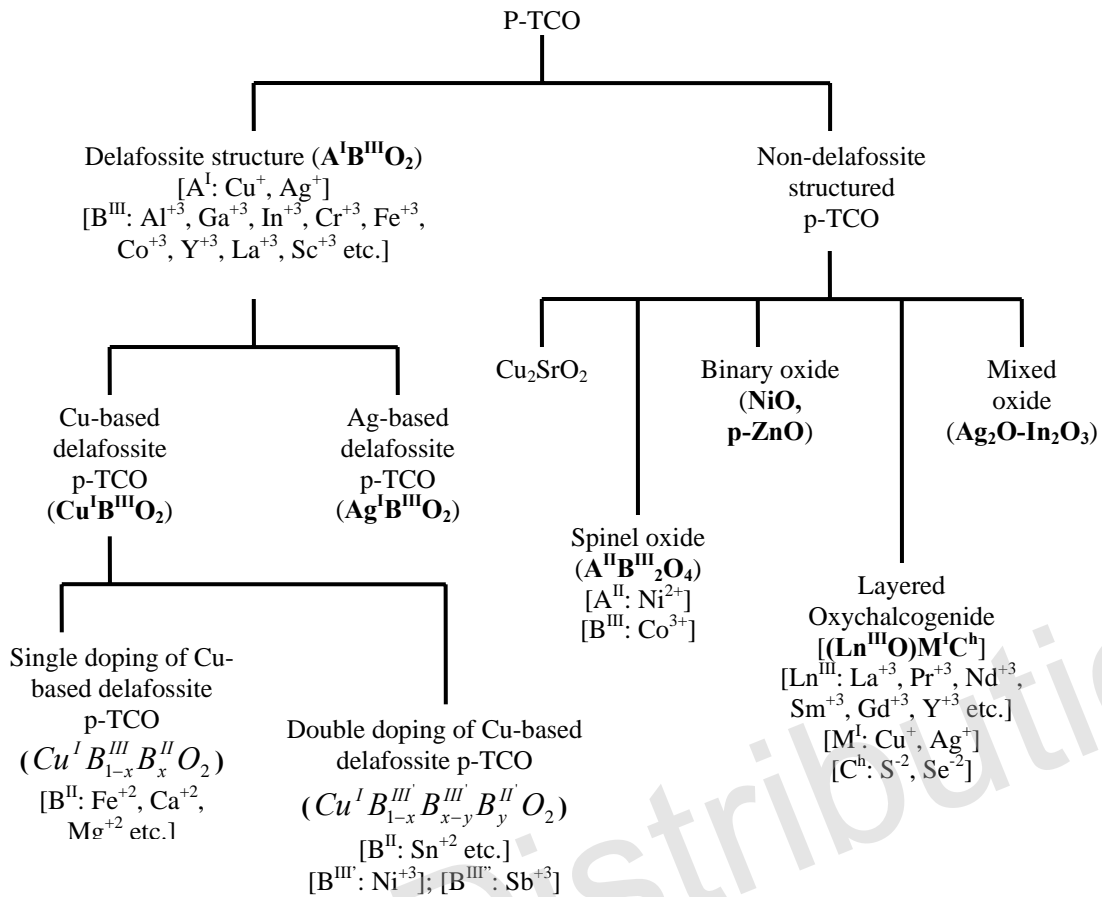


Fig. (2). Chart of various p-TCO materials reported so far. Here the doped versions of Cu-based delafossite p-TCOs have been mentioned only.

Table 1. Delafossite p-TCO thin Films with Different Doping Concentrations and their Respective Opto-Electrical Parameters

Material	Dopant	% of Doping	Average film thickness (nm)	T (%)	E _{g-direct} (eV)	σ _{RT} (S cm ⁻¹)	S _{RT} (μV K ⁻¹)	Ref.
CuAlO ₂	undoped	---	230	70	3.5	0.34	+ 214	102
CuGaO ₂	undoped	---	500	80	3.6	0.063	+ 560	66
CuGa _{1-x} Fe _x O ₂	Fe	0.5	150	60	3.4	1.0	+ 500	69
CuIn _{1-x} Ca _x O ₂	Ca	0.07	170	70	~ 3.9	0.028	+ 480	67
CuCrO ₂	undoped	---	250	40	~ 3.1	1.0	---	71
CuCr _{1-x} Mg _x O ₂	Mg	0.5	270	50	3.1	220.0	+ 150	71, 73
CuYO ₂	undoped	---	200	60	~ 3.5	0.025	---	72, 73
CuY _{1-x} Ca _x O ₂	Ca	0.01–0.02	240	50	3.5	1.05	+ 275	72, 73
CuScO ₂ ^a	undoped	---	110	40	~ 3.3	30.0	---	70, 73
CuSc _{1-x} Mg _x O ₂ ^b	Mg	0.05	220 - 250	80	3.3–3.6	~ 0.07	---	69, 134
				60	-do-	~ 0.1	---	
				25	-do-	~ 0.8	---	
				15	-do-	~ 20.0	---	

(Table 1) Contd....

Material	Dopant	% of Doping	Average Film Thickness (nm)	T (%)	$E_{g-direct}$ (eV)	σ_{RT} ($S\ cm^{-1}$)	S_{RT} ($\mu V\ K^{-1}$)	Ref.
CuNi _{1-x} Sb _x Sn _y O ₂	Ni	0.66	~ 200	60	3.4	0.05	+ 250	69
	Sb	0.33						
	Sn	0.033						
AgCoO ₂ ^c	undoped	---	150	50	4.15	0.2	+ 220	69

^aMaximum of 25 % oxygen was intercalated.

^bThe variation of transparency of the films at the expense of conductivity was due to a variation of oxygen pressure from 3 Torr (for most transparent film) to 15,000 Torr (for least transparent film). Also according to Ref. [189] the doping concentration of Mg was 1 %.

^cThe Ag : Co ratio was 1.1 : 1.

Table 2. Non-Delafossite p-TCO thin Films with Different Doping Concentrations and their Respective Opto-Electrical Parameters

Material	Dopant	% of Doping	Average film thickness (nm)	T (%)	$E_{g-direct}$ (eV)	σ_{RT} ($S\ cm^{-1}$)	S_{RT} ($\mu V\ K^{-1}$)	Ref
Cu ₂ SrO ₂	undoped	---	150	75	~ 3.3	0.004	260	78
Cu ₂ Sr _{1-x} K _x O ₂	K	0.03	120	75	~3.25	0.05	260	76
NiCo ₂ O ₄	undoped	---	100	~ 65	---	~ 16.67	---	77
(LaO)CuS	undoped	---	150	70	~ 3.1	6.4×10^{-5}	713	79
(La _{1-x} Sr _x O)CuS	Sr	0.03	150	60	~ 3.1	20	44	79
(LaO)CuS _{1-x} Se _x	Se	0.0	~ 150	~ 60	> 3.1	~ 0.6	~ 250	86
		0.25				~ 2.5	~ 200	
		0.4				~ 20	~ 250	
		0.7				~ 15	~ 150	
		1.0				~ 25	~ 250	
(La _{1-x} Mg _x O)CuSe	Mg	0.0	~ 150	---	---	24	---	86
		0.2				140 ^d	---	
In ₂ O ₃ -Ag ₂ O ^e	---	---	300	~ 20	---	100	---	90
NiO ^f	undoped	---	111	40	~ 3.8	7.0	---	64
p-ZnO	Ga & N codoped	*	---	~ 90	---	0.23	---	101

^d The film showed degenerate p-type semiconductivity.

^e The film contained 50 wt % Ag₂O.

^f Data given for the films deposited under an atmosphere of Ar + 50 vol. % O₂.

* N : Ga ratio was 2 : 1 with 5 wt % codoped Ga in the film.

Table 3. Deposition Parameters of Different p-TCO Films Grown by PLD Technique

	CuAlO ₂	CuGaO ₂	CuInO ₂ : Ca	CuScO ₂	Cu ₂ SrO ₂ : K	ZnO: N
Laser	KrF (248 nm)	KrF (248 nm)	KrF (248 nm)	KrF	KrF (248 nm)	ArF
Laser frequency (Hz)	20	20	20	1	2	1
Laser power (J cm⁻² pulse⁻¹)	5	6	3.5	1.1	2.5	0.5
Base pressure (Pa)	1 x 10 ⁻⁷	6 x 10 ⁻⁶	1 x 10 ⁻⁷	---	1 x 10 ⁻⁶	1 x 10 ⁻⁶
O₂ pressure (Pa)	1.3	9	1	1.5	7 x 10 ⁻⁴	#
Target	CuAlO ₂ Pellet	CuGaO ₂ pellet	CuInO ₂ : Ca pellet	Cu ₂ Sc ₂ O ₅ pellet	Cu ₂ Sr _{0.97} K _{0.03} O ₂ pellet	ZnO: Ga pellet
Substrate	α-Al ₂ O ₃ (001)	α-Al ₂ O ₃ (001)	α-Al ₂ O ₃ (001)	α-Al ₂ O ₃ (1120)	SiO ₂	SiO ₂
Substrate-target distance (mm)	25	25	25	40	40	---
Substrate Temperature (°C)	690	700	450	900	300	400
Deposition time (min)	---	---	---	---	180	---
Post annealing time (min)	180	none	none	none	120	---
Post annealing temp (°C)	690	none	none	none	300	---
Reference	103, 102	103, 66	67	105	103, 76	101

#The deposition atmosphere was N₂ or N₂O.

Table 4. Different Deposition Parameters of p-TCO Films Synthesized by R.F. Magnetron Sputtering Technique

Material	CuAlO ₂	CuGaO ₂ : Fe	CuCrO ₂ :Mg	CuNi _{2/3} Sb _{1/3} O ₂ :Sn	AgCoO ₂	NiCo ₂ O ₄	(LaO)CuS	NiO	In ₂ O ₃ -Ag ₂ O
R.F. power (W)	65	80	90	80	80	200	110	50	40
Electrode distance (mm)	40	30	38	---	30	---	35	--	---
Base pressure (Pa)	---	---	9.3 x 10 ⁻⁴	---	---	1.33x10 ⁻⁴	---	--	---
Sputtering pressure (Pa)	4.53 (O ₂ press)	13.33 (Ar : O ₂ = 4 : 1)	1.33 (Ar press)	13.33 (Ar:O ₂ = 4:1 / 9:1)	53.33 (Ar:O ₂ = 4:1)	1.33	13 (Ar : H ₂ S = 19 : 1)	0.8 (O ₂ press)	0.25 (Ar + O ₂)
Target	CuAlO ₂ pellet	CuGa _{0.5} Fe _{0.5} O ₂ Pellet	CuCr _{1-x} MgO ₂ pellet	CuNi _{0.67} Sb _{0.3} - - Sn _{0.03} O ₂ pellet	AgCoO ₂ pellet	Co-Ni alloys	(LaO)CuS : Sr pellet	NiO pellet	In ₂ O ₃ -Ag ₂ O pellet
Substrate	α-Al ₂ O ₃ (001)	fused silica	fused quartz	SiO ₂ , YSZ(100), Al ₂ O ₃ (001)	SiO ₂ , Al ₂ O ₃	Quartz, sapphire, Si	SiO ₂	SiO ₂	SiO ₂
Substrate temp. (°C)	ambient	100 °C	450-750	500 °C	400 °C	ambient	ambient	200	ambient
Post-annealing time (min)	90	90	2.5 (RTA in Ar)	180	---	---	120	none	60

(Table 4) Contd....

Material	CuAlO ₂	CuGaO ₂ : Fe	CuCrO ₂ :Mg	CuNi _{2/3} Sb _{1/3} O ₂ :Sn	AgCoO ₂	NiCo ₂ O ₄	(LaO)CuS	NiO	In ₂ O ₃ -Ag ₂ O
Post-annealing temp. (°C)	1050 [§]	800 °C (N ₂ atmos.)	600-900	900 °C (in air)***	---	---	800**	none	500
Reference	104	69	71	69, 74	69	78	79	64	90

[§] *Ex situ* in a Lindberg box furnace containing small amount of CuAlO₂ powder.

** *Ex situ* in an evacuated silica tube containing small amount of (LaO)CuS powder.

*** Also for some cases RTA in air at 900 °C was performed.

Table 5. Various Parameters Used to Deposit Different p-TCO Films by R. F. Magnetron Reactive Sputtering Technique

Material	Cu-Al-O films (a mixture of CuAlO ₂ and CuO)	p-ZnO
R. F. power (W)	Al power - 60 to 110 [‡] Cu power - 30 W	20
Targets	metallic Cu and Al	Metallic Zn
Substrate	glass	Si (1 0 0)
Substrate temperature (°C)	100	350
Sputtering atmosphere	Ar + 5% O ₂	Ar + 83 %O ₂ (pressure ~ 4 Pa)
Post annealing	none	At 750 °C, in vacuum (~ 1.33 x 10 ⁻⁴ Pa), for 30 min.
Reference	[112]	[147]

[‡] For Al power 110 W single phase amorphous CuAlO₂ was formed

Table 6. Deposition Parameters of Reactively d.c. Sputtered p-CuAlO₂ Thin Films

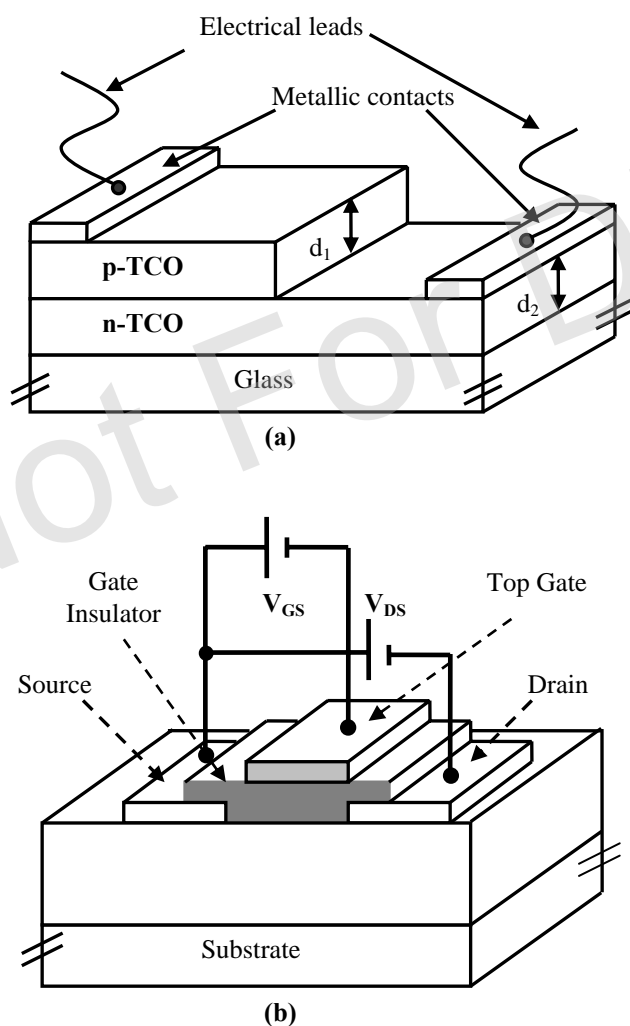
Material	CuAlO ₂ thin film	CuAlO ₂ thin film	CuAlO ₂ thin film*
Target	Elemental Cu & Al metal (facing) targets	Mixture of Cu + Al metal powder pellets	Cu / Al alloy (with 1:3 ratio)
Electrode distance (mm)	-----	18	65
Sputtering Voltage (V)	Cu facing targets = 750V Al facing targets = 350 V	1000	292 - 394
Current density (mA cm ⁻²)	Cu facing targets ~ 1.17 Al facing targets ~ 7.0	12	200 - 300 mA (current)
Base pressure (Pa)	-----	10 ⁻⁴	5 x 10 ⁻⁴
Sputtering pressure (Pa)	0.53	20.0	4.0
Sputtering atmosphere	Ar + O ₂ (4 : 1)	Ar + O ₂ (3 : 2)	Ar + O ₂
Substrate	quartz (rotating)	Si (400) & glass	glass
Substrate temperature (°C)	300	200	250
Deposition time (min)	240	240	----
Post annealing time (min)	240	120	----
Post-annealing temp. (°C)	> 700	220	----
Post annealing atmosphere	N ₂ (ambient pressure)	O ₂ (20 Pa)	-----
Reference	[113]	[114]	[117]

*This process involved d.c. reactive magnetron sputtering technique.

Table 7. Deposition Parameters for Various Co-Evaporation Techniques for the Deposition of p-TCOs

Material	CuYO ₂ : Ca*	CuGaO ₂	BaCuSF
Reactants	Elemental Cu, Y, Ca metals	Cu, Ga metals	Cu metal, BaF ₂
Base pressure (Pa)	9.33 x 10 ⁻⁵	9.33 x 10 ⁻⁵	---
Reactant gas	O ₂	O ₂	H ₂ S
Deposition pressure (Pa)	0.02	0.02	---
Substrate	Glass, MgO (100), Si	SiO ₂	SiO ₂ , MgO
Substrate temperature (°C)	80 - 650	100	200
Post annealing time (min)	3 (RTA)	90	180
Post annealing temp. (°C)	600	800	350
Post annealing atmosphere	O ₂	N ₂	H ₂ S
Reference	72	69	134

* 1-2 % Ca doping in Y - sites

**Fig. (3).** Schematic diagram of (a) an all-TCO p-n junction diode on glass substrate, (b) a top-gated TFET structure [154].

nanoparticles, the research on nanostructured materials generates great interest in the scientific community and offers tremendous opportunities in science and technology because of new properties exhibited by these materials and challenging problems thrown up for providing theoretical concepts in physics associated with it [158-160]. In fact, both the natural as well as the artificial world can now be categorized in two regimes: micro regime and nano regime. Starting from a human hair to DNA structure - the nature evolves itself from micro to nano scale structures. Similarly, man made world is now shifting its attention from micro devices to nano materials. Fig. (4) schematically represents the broad spectrum of the micro and nano regime, indicating how natural and man made world evolve into smaller domain.

Optical properties of nanocrystals are markedly related to their size and surface chemistry and drastically differ from those of bulk materials. Preparation and study of high quality quantum dots, nanobelts and nanowires [161-163] have been reported widely. These achievements in the last few years have focused nanoparticle research on their applications in electrical and optoelectronics devices [164-165]. But most of the commercially available devices fabricated by nano-materials are passive nano-devices, whereas fabrication of nano-active devices is still under research level. But, with the recent exponential growth and development in the nanotechnology, it is just a matter of time to realize commercially viable high-efficient nano-active devices. In fact, the recent report of the U.S. National Nanotechnology Initiative, showed that the growth of the nanotechnology can be divided into four generations (shown in Fig. (5)). The current era, is that of passive nanostructures, materials designed to perform one task. The second phase, which we are just entering, introduces active nanostructures for multitasking; for example, diodes, transistors, actuators, drug delivery devices, and sensors. The third generation is expected to begin emerging around 2010 and will feature nanosystems with thousands of interacting components. A few years after that, the first integrated nanosystems,

Table 8. Various Parameters of Deferent All-Transparent Diodes

Diode structure		p-NiO/i-NiO/ i-ZnO/ n-ZnO:Al	n-ZnO/ p-SrCu ₂ O ₂	n-ZnO/ p-SrCu ₂ O ₂ : K	n-ZnO:Al/ p-CuYO ₂ :Ca	n-ZnO/ p-CuAlO ₂	n-CuInO ₂ : Sn/ p- CuInO ₂ : Ca	n-ZnO: Al/ p-ZnO: As	n-ZnO/ p-ZnO
Thickness (nm)	<i>p-layer</i>	195	300	200	300	400	400	1500-2000	5000
	<i>i-layer</i>	216	---	---	---	---	---	---	---
	<i>n-layer</i>	400	300 - 1000	200	250	400	400	600	5000
Carrier concentration (cm ⁻³)	<i>p-layer</i>	10 ¹⁹	10 ¹⁷	~10 ¹⁸	---	---	---	---	~ 5 x 10 ¹⁵
	<i>n-layer</i>	7 x 10 ²⁰	5 x 10 ¹⁸	~10 ¹⁸	---	---	---	---	~ 6 x 10 ¹⁵
Substrate		Glass	Glass	YSZ (111)	Glass	Glass	YSZ (111)	GaAs (001)	Si (100)
Deposition technique	<i>p-layer</i>	R. F. magnetron sputtering	Reactive co- evaporation in O ₂ atmosphere	PLD	Reactive co- evaporation in O ₂ atmosphere	PLD	PLD	R. F. Magnetron sputtering	R. F. Magnetron reactive sputtering
	<i>i-layer</i>	R. F. magnetron sputtering with post- annealing in air(at 300°C)	---	---	---	---	---	---	---
	<i>n-layer</i>	---	Magnetron sputtering	PLD	R. F. Magnetron sputtering	PLD	PLD	R. F. Magnetron sputtering	R. F. Magnetron reactive sputtering
Electrodes	<i>p-side</i>	Al	ITO	Ni	In	ITO	ITO	In	Au/Al
	<i>n-side</i>	Al	n ⁺ -ZnO	ITO	ITO	n ⁺ -ZnO	ITO	In	Au/Al
Turn-on voltage (V)		~1.5	~ 0.5	~ 1.0	0.4 – 0.8	0.4 – 1.0	1.8	~ 2.5	~ 1.0
Diode factor		---	1.62	---	---	---	---	---	---
Reference		64	137	138	72	143	68	146	136

Table 9. Different Growth Techniques and Parameters of TFETs

Active Channel	Gate Insulator	Back Gate Electrode	Substrate used	Mobility (cm ² V ⁻¹ s ⁻¹)	On/Off ratio	Visible Transparency (%)	Reference
SnO ₂ : Sb (Thickness ~ 110 nm) (Deposition technique: PLD)	PbZr _{0.2} Ti _{0.8} O ₃ (Thickness ~ 160 nm) (Deposition technique: PLD)	SrRuO ₃ (Thickness ~ 140 nm) (Deposition technique: PLD)	SrTiO ₃ (100)	10.0	~ 10 ⁴	Transparent, as seen in the figure provided, but no numerical data given.	149*, 150

(Table 9) Contd...

Active Channel	Gate Insulator	Back Gate Electrode	Substrate used	Mobility ($\text{cm}^2\text{V}^{-1}\text{s}^{-1}$)	On/Off ratio	Visible Transparency (%)	Reference
ZnO (Thickness ~ 100 nm) (Deposition technique: PLD)	$\text{Al}_2\text{O}_3 + \text{TiO}_2^\#$ (Thickness ~ 220 nm) (Deposition technique: ALD)	ITO (Thickness ~ 200 nm) (Deposition technique: Sputtering)	Glass	2.5	$\sim 10^7$	75	151
ZnO (Thickness ~ 140 nm) (Deposition technique: PLD)	$\text{SiO}_2 + \text{SiN}_x^\ddagger$ (Thickness ~ 250 & 50 nm respectively) (Deposition technique: PECVD)	ITO (Thickness ~ 100 nm) (Deposition technique: e-beam evaporation)	Glass	1.0	10^5	80	152
$\text{InGaO}_3(\text{ZnO})_5^\ddagger$ (Thickness ~ 120 nm) (Deposition technique: PLD)	a-HfO ₂ (Thickness ~ 80 nm) (Deposition technique: PLD)	ITO (Thickness ~ 30 nm) (Deposition technique: PLD)	YSZ (111)	80.0	$\sim 10^6$	80	154 ^{††}

* Due to the presence of ferroelectric insulator $\text{PbZr}_{0.2}\text{Ti}_{0.8}\text{O}_3$, the device showed intrinsic memory function.

$\text{Al}_2\text{O}_3 + \text{TiO}_2$ is an alternative layers of Al_2O_3 & TiO_2 .

† This TFET has a double layer Gate insulator.

‡ Single-crystalline $\text{InGaO}_3(\text{ZnO})_5$ is used as active channel layer.

†† The device has top-gate structure.

functioning much like a mammalian cell with hierarchical systems within systems, are expected to be developed.

In this context, transparent nano-active devices will be very interesting and important field of research in nanotechnology. Syntheses and characterizations of nanostructured n-TCOs are very important and well-established field in nanotechnology and still growing in stature. Therefore, the formation of nanocrystalline p-type counterpart may open up an extremely important and interesting field of research for the fabrication of all-transparent nanoactive devices. This will not only give a new dimension in the field of "Transparent Nano-Electronics", but new avenues may open up in the nanoparticle research keeping an eye on its tremendous applications in optoelectronics technology.

2. DIFFICULTIES IN OBTAINING P-TCO AND POSSIBLE REMEDIES

2.1. Chemical Modulation of the Valence Band

It has been observed that the preparation of binary metal oxides with p-type conductivity is very challenging and that is why, most of the existing TCOs are n-type in nature. The possible reason is the electronic structure of these metal

oxides, where strong localization of holes (introduced by intentional substitutional doping) at oxygen 2p levels or an upper edge of the valence band due to high electronegative nature of oxygen, i.e. this localization is due to the ionicity of metallic oxides [65, 103]. O 2p levels are far lower lying than the valence orbit of metallic atoms [166], leading to the formation of deep acceptor level by the holes. In other words, the holes, therefore, have high probability to be localized around the oxygen atoms. Hence these holes require high enough energy to overcome large barrier height in order to migrate within the crystal lattice, resulting in poor conductivity and hole mobility. A possible solution proposed by Kawazoe and co-authors [103] is to introduce a "degree of covalency" in the metal-oxygen bondings to induce the formation of an extended valence band structure, i.e. the valence band edge should be modified by mixing orbitals of appropriate counter cations that have energy-filled-levels comparable to O 2p level. This would reduce the strong coulombic force by oxygen ions and thereby delocalizing the holes. This is the essential approach to obtain p-TCO, which is called "Chemical Modulation of the Valence Band (CMVB)" [103].

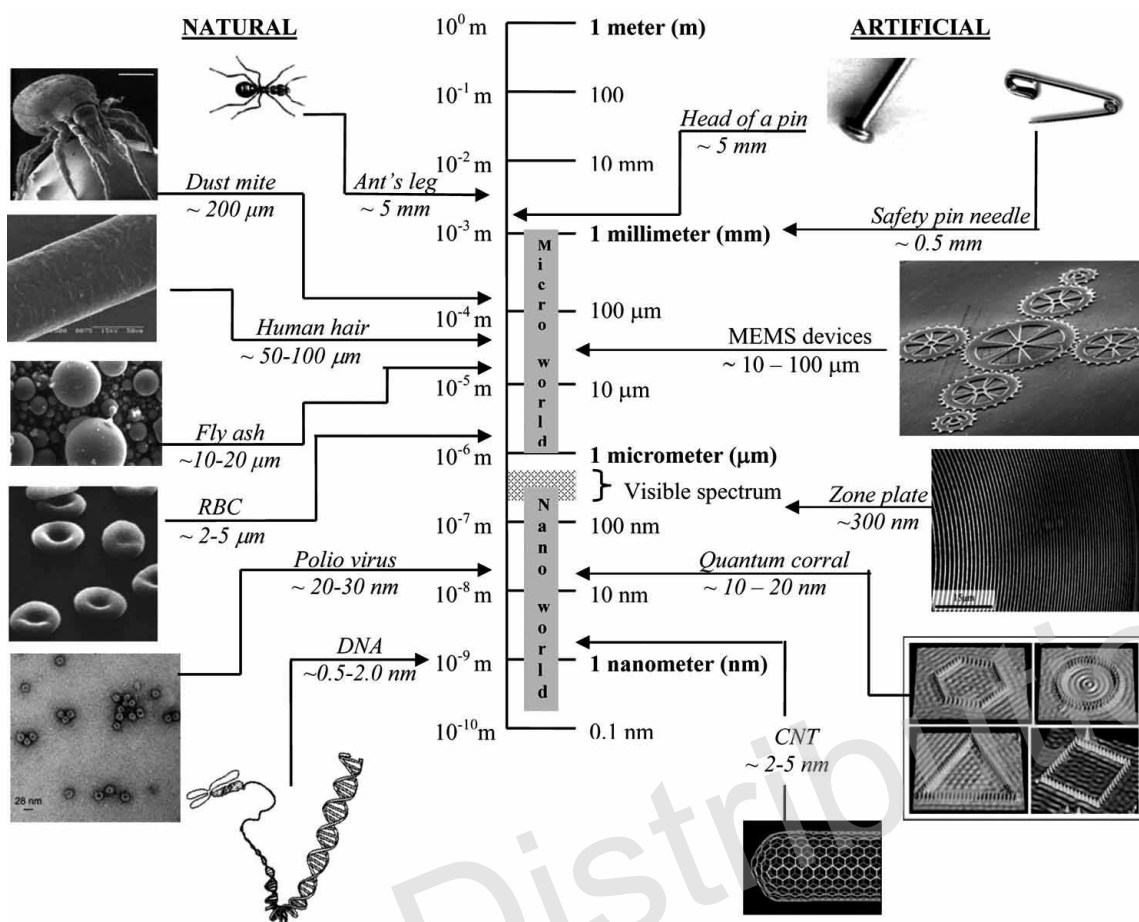


Fig. (4). Description of nano regime. From Forbes-Nanotech Report.

But the next requirement is the choice of appropriate cationic species that will serve for CMVB technique. Investigations showed that the required cationic species are $3d^{10}$ -closed shell of Cu^+ ions and $4d^{10}$ -closed shell of Ag^+ ions [103, 166]. Although some transition metal cations with open d-shell may fulfill the energy requirement [167] for CMVB technique, but they usually show strong coloration due to d-d transition, which is not expected for transparent materials. Hence focus had been concentrated on the cations mentioned above, with closed ($d^{10}s^0$) electronic configuration. Fig. (6) shows a schematic illustration of CMVB technique. Both of the atomic orbitals are occupied by electron pairs, and the resulting antibonding level becomes the highest occupied level, i.e. the valence band edge.

Next is the structural requirement for designing p-TCO materials. Tetrahedral coordination of oxide ions is advantageous for p-type conductivity, as it acts in reducing the localization behavior of 2p electrons on oxide ions [103]. The valence state of the oxide ions can be expressed as sp^3 in this conformation. Eight electrons (including $2s^2$) on an oxide ion are distributed in the four σ bonds with the coordination cations. This electronic configuration reduces the non-bonding nature of the oxide ions and increases the delocalization of holes at the valence band edge (that is why Cu_2O is a p-type conducting oxide [168-170]). But Cu_2O , although p-type in nature, has rather small bandgap (2.17 eV) [169]. This is probably because of the three-dimensional

interactions between $3d^{10}$ electrons of neighboring Cu^+ ions. It is expected that the low-dimensional crystal structure would suppress this interaction [102]. As we are interested in transparent conducting oxides, bandgap of the material (E_g) should be greater than 3.1 eV. Hence, enlargement of bandgap would be another structural requirement for designing p-TCO, so that there is no absorption of visible photons. Materials with delafossite crystal structure $\text{A}^I\text{B}^{III}\text{O}_2$ (A^I = Monovalent ions, Cu^+ , Ag^+ ; B^{III} = Trivalent ions, Al^{3+} , Ga^{3+} , In^{3+} , Cr^{3+} , Fe^{3+} , Co^{3+} , Sc^{3+} , Y^{3+} etc.) [171-173] were chosen as the candidates for p-TCOs for several reasons. Firstly, if we investigate the delafossite structure as shown in Fig. (7), we see an alternative stacking of A^I and layers of nominal B^{III}O_2 composition consisting $\text{B}^{III}\text{-O}_6$ octahedra sharing edges. Each A^I atom is linearly coordinated with two oxygen atoms to form a $\text{O-A}^I\text{-O}$ dumbbell unit placed parallel to the c-axis. O-atoms of $\text{O-A}^I\text{-O}$ dumbbell link all A^I layers with the B^{III}O_2 layers. On the other hand, each oxide ion in the B^{III}O_2 layer forms a "pseudo-tetrahedral coordination ($\text{B}^{III}_3\text{A}^I\text{O}$)" [103] with the neighboring B^{III} and A^I ions. Hence, as previously mentioned, this electronic configuration reduces the non-bonding nature of the oxide ions and, therefore, delocalizes the holes at the valence band edge. Secondly, this layered structure ($\text{O-A}^I\text{-O}$ dumbbell layer and B^{III}O_2 layer) effectively reduces the dimension of cross-linking of A^I ions and, thus enlarging the bandgap [65]. And finally, another important factor in this structure is the

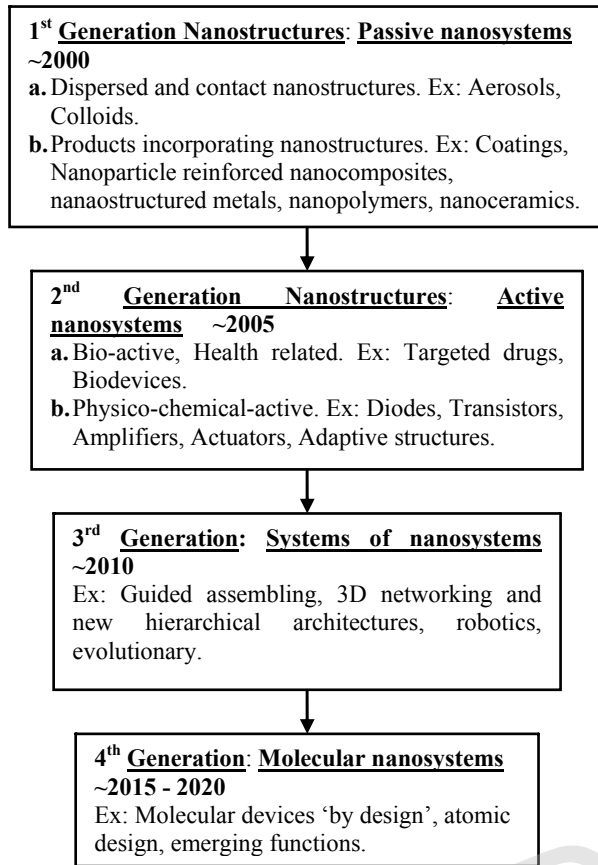


Fig. (5). Roadmap to Nanotechnology (from US National Nanotechnology Initiative report).

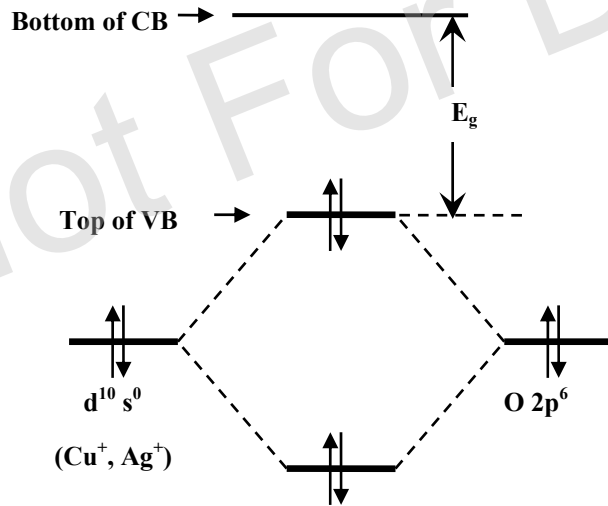


Fig. (6). Schematic diagram of CMVB method. Energy levels are not to the scale [103].

low coordination number of the A^I ions, due to the large separation from oxygen legands, which is the result of the strong coulombic repulsion between 2p electrons in oxygen legands and $A^I d^{10}$ electrons. This leads to the $A^I d^{10}$ energy levels almost comparable to the O 2p level, resulting in a high degree of mixing of these levels, which is essential for CMVB technique [103].

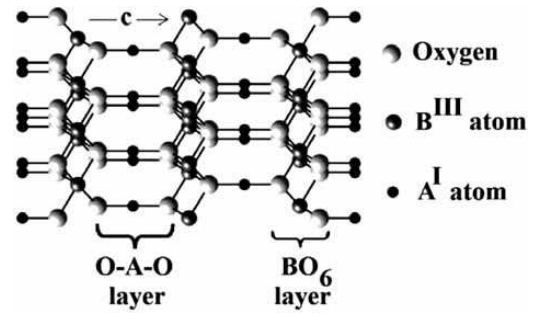
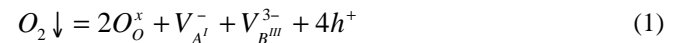


Fig. (7). Delafossite Crystal Structure.

As the importance of p-TCO lies in the active device fabrication, it is very important to have lattice matching between both p and n-types of TCOs to form p-n homojunctions. Both types of TCOs with delafossite structure may serve this requirement. In this regard, it is also worthwhile to mention that the $B^{III}O_2$ layers of this structure is also important for designing n-TCOs, specially for the cations like Ga^{+3} , In^{+3} in the B^{III} sites with s^0 configuration [103]. Following the above argument, delafossite AgInO_2 thin film with n-type semiconductivity had already been established [174].

NONSTOICHIOMETRY AND DOPING IN P-TCO

The cause of p-type conductivity shown by p-type transparent conducting oxide materials is due to excess oxygen (or metal deficit) within the crystallite sites of the material, i.e. the defect chemistry plays an important role. This deviation from the stoichiometric composition of the components can be induced by regulating the preparation condition of the materials. The defect reaction may be represented by the following equation [175,176]:



where 'O_O' denotes the lattice oxygen, 'V' denotes the vacancies of monovalent cation A^I and trivalent cation B^{III} respectively and 'h' denotes the hole. Superscripts \times , -, and + denote effective neutral, negative, and positive charge states respectively. The symbol, \downarrow , denotes the dissolution of oxygen within the material during oxidation.

Also, intercalation of excess O^{2-} ions in the interstitial sites may trap electrons, leaving behind empty states in the valence band, which act as holes. The formula for oxygen-excess delafossite films may be written as $A^I B^{III} O_{2+x}$ ($A^I = \text{Cu}^+, \text{Ag}^+$ and $B^{III} = \text{Al}^{+3}, \text{Ga}^{+3}, \text{In}^{+3}, \text{Y}^{+3}, \text{Sc}^{+3}$ cations etc.). The value of x i.e. the percentage of excess oxygen may be as low as 0.001% in CuAlO_{2+x} thin film [135] to more than 25% in CuYO_{2+x} polycrystalline powder and CuScO_{2+x} thin films [73, 177-179]. Fig. (8-i), (8-ii) and (8-iii) show schematic representation of stoichiometric $A^I B^{III} O_2$ crystal and non-stoichiometric $A^I B^{III} O_{2+x}$ crystal with "excess" oxygen in lattice sites and interstitial sites.

Oxygen intercalation in delafossite p-TCOs only showed a maximum reported conductivity around $3 \times 10^1 \text{ S cm}^{-1}$ [70]. But this is still quite less than that of commercially available n-TCOs like indium tin oxide (ITO), which is having room temperature conductivity more than $1 \times 10^3 \text{ S cm}^{-1}$. So next attention was focused on the substitutional

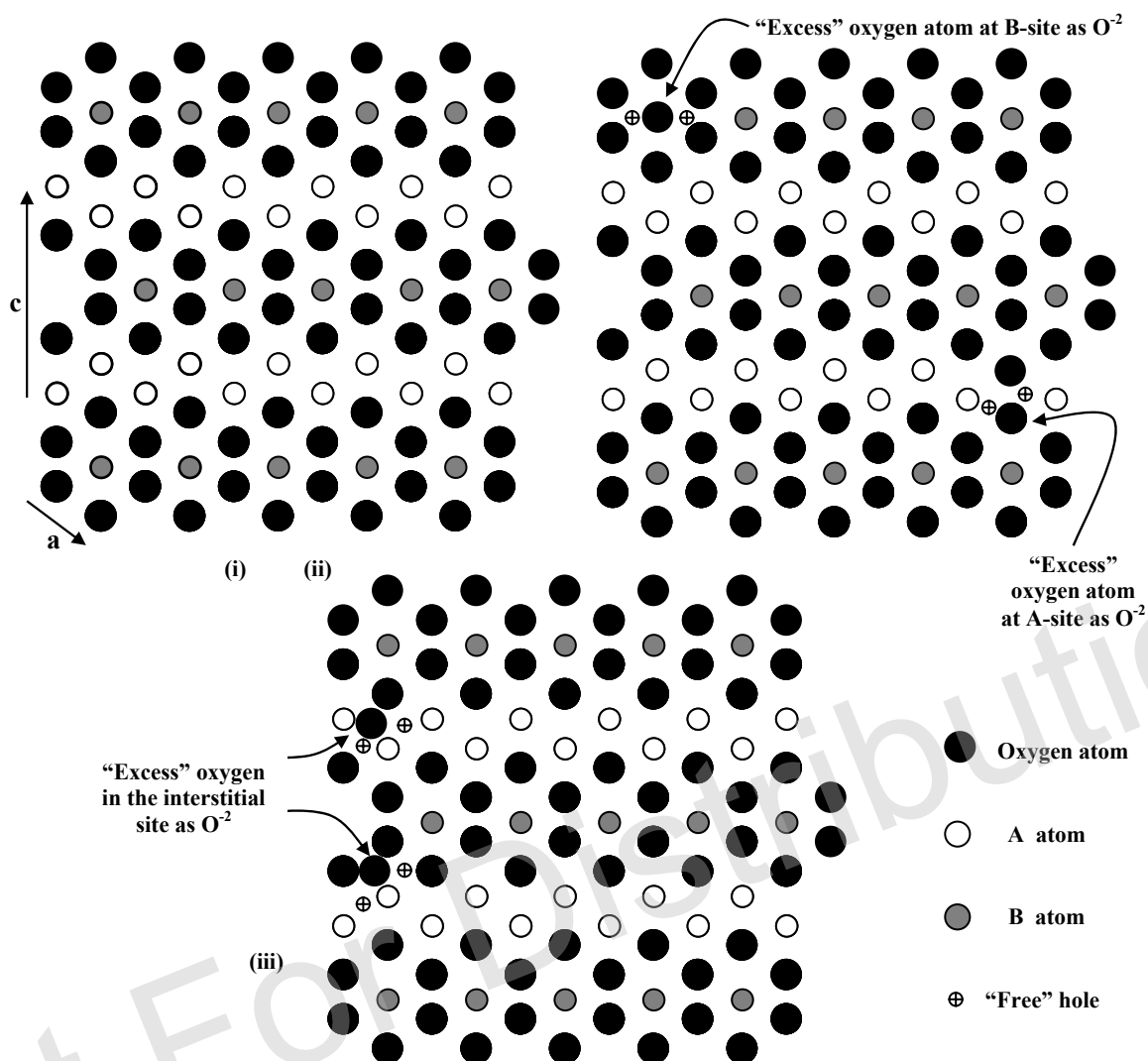
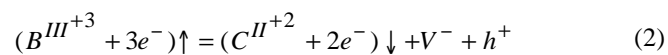


Fig. (8). Schematic diagram of (i) Stoichiometric ABO₂ lattice, (ii) Non-stoichiometric ABO_{2+x} structure with "excess" oxygen in lattice sites, (iii) interstitial sites. The diagram is not according to the relative lattice parameters.

doping of these materials by appropriate dopants to increase the conductivity. Doping of CuAlO₂ was first attempted, as it was the first reported material amongst p-TCO thin films [65]. Several groups theoretically calculated the effects on the electronic behavior of the material due to the presence of various cations in Cu and (or) Al sites. Lalić and co-authors [180-181] showed that Cd and Zn substitutions on Cu site would produce n-type conductivity in the material, whereas Ni doping in Cu sites would enhance the p-type conductivity of the material. But Cd doping on Al sites would have no effect on the electrical properties of the material. Preparation of a solid solution of gallium doped copper aluminum oxide in the form of CuAl_{1-x}Ga_xO₂ (0 ≤ x ≤ 0.5) was reported by Shahriari *et al* [129]. But no film preparation of this material was reported by them. Also any other experimental data on the doping of CuAlO₂ thin film has not been reported yet. Heavy doping (~ 50 %) of CuGaO₂ by Fe⁺³ in Ga sites has been reported by Tate *et al.* [69]. Their strategy was to combine high transparency of CuGaO₂ thin film (~ 80% in visible region [66]) with better conductivity (over other Cu and Ag based delafossites [173]) of CuFeO₂ pellets (2.0 S

cm⁻¹ [173, 182]). Both the polycrystalline powder and thin film of CuGa_{1-x}Fe_xO₂ (0 ≤ x ≤ 1) have shown p-type conductivity. It was observed that high Fe doping had increased the conductivity of the film from 2 × 10⁻² S cm⁻¹ (for undoped CuGaO₂ thin film) to almost 1.0 S cm⁻¹ for CuGa_{1-x}Fe_xO₂ (x = 0.5) thin film, whereas transparency of the films became ~ 60 % in the visible region [69]. Doping of CuInO₂, CuYO₂, CuScO₂, CuCrO₂ by divalent cations e.g. Ca⁺², Mg⁺² etc. were reported by various groups [67-72]. When a trivalent cation was replaced by a divalent one, one empty state in the valence band was created, which acts as a hole, thus increasing hole conductivity. The method may be described by the following equation:



where B^{III+3} and C^{II+2} are trivalent and divalent cations, V⁻ is the vacant state occupied by an electron, e⁻ and h⁺ is a "free" hole. The symbols ↑ and ↓ denote the replacement of trivalent cation by divalent one in the lattice sites. Such

doped delafossite films like $\text{CuCr}_{1-x}\text{Mg}_x\text{O}_2$ ($x = 0.05$), $\text{CuY}_{1-x}\text{Ca}_x\text{O}_2$ ($x = 0.01 - 0.02$), $\text{CuSc}_{1-x}\text{Mg}_x\text{O}_2$ ($x = 0.05$) showed better hole conductivity over the corresponding undoped films [71]. Some Ag based delafossite materials like $\text{AgM}^{\text{III}}\text{O}_2$ ($\text{M}^{\text{III}} = \text{Sc}^{+3}, \text{Cr}^{+3}, \text{Ga}^{+3}$ etc.) with 5% Mg doping at M^{III} sites was reported by Nagrajan *et al.* [73]. The conductivities of these sintered powders were very low ($\sim 10^{-5} - 10^{-4} \text{ S cm}^{-1}$) and also no film preparation of these materials were reported anywhere so far.

There are also reports in the literature about the double substitution of trivalent M^{III} sites by divalent and pentavalent cations e.g. $\text{CuFe}_{1-x}\text{V}_x\text{O}_2$ ($x = 0.5$), $\text{CuNi}_{1-x}\text{Sb}_x\text{O}_2$, $\text{CuZn}_{1-x}\text{Sb}_x\text{O}_2$, $\text{CuCo}_{1-x}\text{Sb}_x\text{O}_2$, $\text{CuMg}_{1-x}\text{Sb}_x\text{O}_2$, $\text{CuMn}_{1-x}\text{Sb}_x\text{O}_2$ ($x = 0.33$), $\text{AgNi}_{1-x}\text{Sb}_x\text{O}_2$, $\text{AgZn}_{1-x}\text{Sb}_x\text{O}_2$ ($x = 0.33$) etc., but all in the form of sintered powder [74, 183]. Also triple substitution of trivalent cation had been reported by Tate and co-authors [69, 74] in the form of $\text{CuNi}_{1-x}\text{Sb}_x\text{Sn}_y\text{O}_2$ ($x = 0.3$, $y = 0.033$). Thin film of this material showed an average of 60 % transmittance with a room temperature conductivity of $5 \times 10^{-2} \text{ S cm}^{-1}$. The exact electronic structure and conduction mechanism of these types of materials are yet to be explored completely.

3. RECENT REVIEW AND PATENTING ACTIVITIES IN NANO/MICRO-STRUCTURED P-TCO

For new materials with novel properties and applications, patent generation is an important but common practice within scientific communities. As p-TCO is a new and interesting group of materials with important applications in the new field of "Invisible Electronics", there are no exceptions of filing patents on various aspects of this new group of materials. Although Shannon, Sato, Kawazoe, Thomas, Wager and co-authors [53, 64, 65, 135, 171-173] first reported the formation of delafossite p-TCOs and possible applications in "Invisible Electronics", Shahriari and co-authors [184] first filed patents on the low-temperature ($< 500^\circ\text{C}$), low-pressure ($< 3 \times 10^8 \text{ Pa}$) preparation of p-type, delafossite-structured, monovalent conducting, phase-pure ABO_2 materials (A: monovalent cations Cu^+ , Ag^+ , Pt^+ , Pd^+ , B: trivalent cations Al^{+3} , Ga^{+3} , Fe^{+3} , La^{+3} , In^{+3} , Sc^{+3} etc.). This group has used stoichiometric amounts metallic A, B and their oxides (e.g. AO , A_2O , B, and B_2O_3) in an FEP (fluoro(ethylenepropylene)) Teflon pouch along with ground NaOH pellets in it. The pouch was sealed and placed in a Teflon-lined autoclave (Parr) filled with deionized water. The autoclave was sealed and first heated to about 150°C for 5 hours to allow H_2O to enter the permeable membrane of the pouch and dissolve the NaOH. This was followed by an approximate heating at 210°C for 48 hours, with subsequent cooling to room temperature at 0.1 to 6°C/hr . Delafossite crystallites were recovered by filtration. A flow-chart of the synthesis of delafossite CuAlO_2 crystallites is shown in Fig. (9). The two-step heating is an important part of the reaction and material formation. The Teflon pouches heated above 100°C become permeable and an exchange reactions occurs between the inside powder and the outside solution. This reaction is very exothermic and appears to be responsible for the two-step heating process. The first step 150°C seems to initialize the reaction, and the second step around

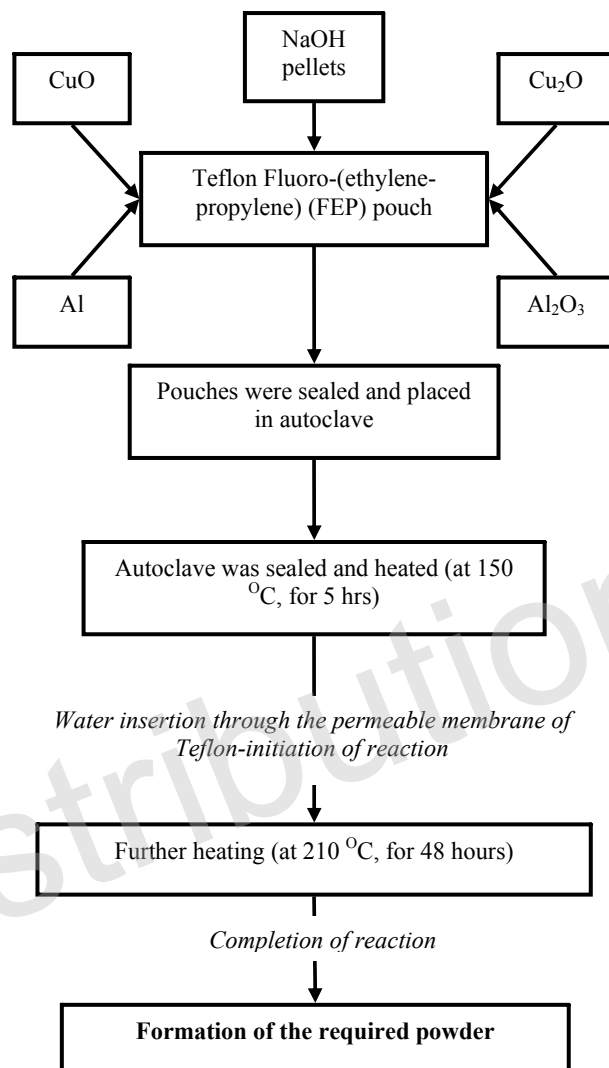


Fig. (9). Flow chart for the hydrothermal synthesis of CuAlO_2 powder [184].

215°C completes it. Previously, Shannon *et al.* [171-173] hydrothermally synthesized several ABO_2 delafossites under extreme conditions of temperature and pressure using platinum or gold tubes. This manifests the higher temperature and pressure for reaction. But in the case of Shahriari and group, the use of Teflon pouch creates the low-temperature, low-pressure condition for reaction as the Teflon becomes permeable around 100°C and initiates the reaction. For the syntheses of silver-based delafossites (AgBO_2), the above-mentioned hydrothermal process appears to be particularly important to grow superior quality materials. Previously, Shannon and co-authors used a multi-step cation exchange method instead of high-temperature solid-state reaction to prepare these types of materials, as silver oxide decomposes around 160°C . Therefore the above-mentioned hydrothermal method appears to be a uniform synthesis route to prepare various types of delafossite materials. The thermo-gravimetric analysis (TGA) of the hydrothermally synthesized samples (shown in Fig. (10)) shows the chemical formula of the material is $\text{CuAlO}_{2.185}$. The excess oxygen intercalation causes the p-type conductivity of the material as described in

previous sections. The temperature variation of conductivity of the as-synthesized powder is shown in Fig. (11), which shows a room-temperature conductivity around $1.3 \times 10^{-3} \text{ Scm}^{-1}$ with an activation energy (corresponds to the minimum energy required to transfer a hole from valence band to the acceptor level, for p-type material) of 93 meV. These values are comparable to that reported previously by Benko and Coffyberg [185] for CuAlO_2 powder pellets ($1.7 \times 10^{-3} \text{ Scm}^{-1}$) and the curve resembles with that reported by Kawazoe *et al.* [65] within the temperature range shown in the figure. Photo-electrochemical measurement depicts the existence of indirect bandgap of the material around 1.65 eV, which resembles with that reported previously [185]. Therefore, this scheme of synthesis procedure given by Shahriari *et al.* [184] provides a general methodology for the hydrothermal preparation of ABO_2 compounds, compositions and/or materials, including entire $\text{A}_{1-m}\text{A}'_m\text{B}_{1-n}\text{B}'_n\text{O}_2$ solid solutions.

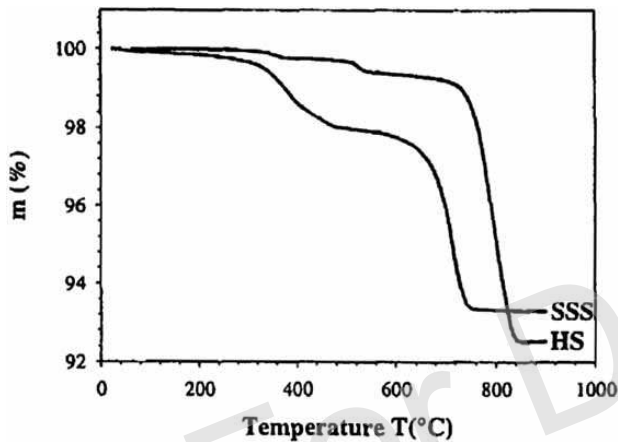


Fig. (10). Comparison of TGA analysis of hydrothermally synthesized (HS) and high-temperature solid-state synthesized (SSS) CuAlO_{2+x} powders [184].

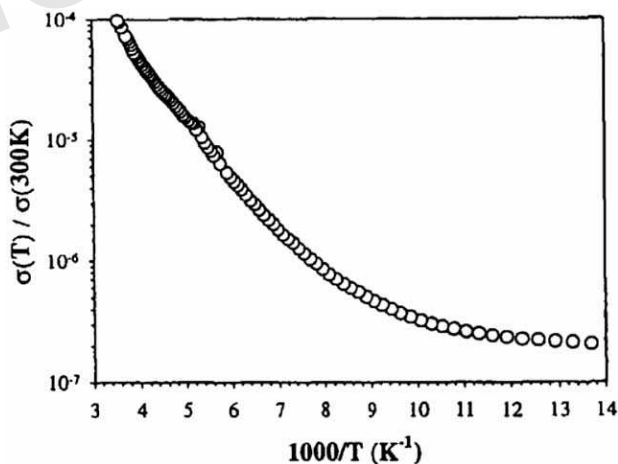


Fig. (11). Temperature variation of conductivity of p- CuAlO_{2+x} powder pellets [184].

Besides p-type delafossite oxides, binary metal oxide such as p-ZnO is another and very important material in p-TCO technology. Doped versions of zinc oxides (ZnO: In/Al/F/B/Ga) are well known and widely used transparent oxides with n-type conductivity [3, 8]. Advent of p-ZnO is an important milestone in "Transparent Electronics" [53, 135] due to the fact that p-n homojunction can be fabricated by both types of zinc oxides, which is a key structure in this field. The attempt to synthesize p-ZnO was first made long back in 1960 by Lander [91] and a decade later by Hümmer [92]. Later considerable efforts were made to produce p-ZnO doped with N [93-98, 186-191] and As [99], Sb [192], P [193] etc. But theoretical calculations of the electronic band structure predicted that nitrogen is the best candidate for producing a shallow acceptor level in ZnO [194, 195]. However, to substitute oxygen by nitrogen, the use of source species that contain only one nitrogen atom per entity (NH_3 , NO, N, NO_2) should be more amenable to acceptor-state formation because of the large dissociation energy of N_2 (9.9 eV) [196]. Recently, from first principle calculation, Yamamoto and co-authors [100] proposed that 'co-doping' of donor - acceptor dopants (e.g. Ga and N respectively) in ZnO might lead to p-type ZnO. Successful fabrication of p-ZnO by this theory has been realized first by Joseph and co-authors [101]. In this method the simultaneous doping of both acceptor (N) and donor (Ga) into ZnO lattice were done with an acceptor concentration twice that of donor concentration to get maximum conductivity in p-ZnO. The essential approach of this method is to stabilize the N substitution in the appropriate ZnO lattice sites by formation of N-Ga-N type bonds, which would reduce the N-N repulsive interaction (Madelung Energy) and thereby making the acceptor level shallower, thus enhancing the acceptor doping [100, 101]. Following this notion, Zhang and co-authors [197] reported the fabrication of N-Al co-doped p-ZnO films by solution-based technique. But later, several reports pointed out on the reproducibility of p-ZnO and difficulties in 'co-doping' technique [198,199]. Although this put some questions on 'co-doping' theory, but non-realization of proper growth parameters as well as formation of some non-ZnO species in the ZnO matrix in these studies may not be ruled out which shows unambiguous results. Recently, few groups reported the possibility of fabricating p-ZnO with metallic Na and Mn as the dopant source [200-201]. Also Tan *et al* [202] fabricated intrinsic p- ZnO_{1+x} by controlling the Zn: O ratio within the material. This report is important in the sense that p-n homojunction can be fabricated by controlling only the oxygen atmosphere inside the growth chamber without the hassle of intentional substitutional doping. Recently, Triboulet and Perrière [203] reviewed the advancement in the field of ZnO films and briefly described the importance and recent status of p-ZnO films. Similarly, Dai and co-authors [204] reviewed the recent advances in the field of p-ZnO thin film. These review works dealt in details with the various growth techniques of both n- and p-type epitaxial ZnO films and their device applications in optoelectronics, spintronics etc. These reports and the corresponding references therein would provide an in-depth knowledge in the development of p-ZnO thin films. Tremendous scopes lie ahead in this area of research for future applications.

As far as patenting activities of p-ZnO is concerned, Yan and Zhang [205] filed patent for providing a method of fabricating N-doped ZnO with high hole conductivity. The deposition is done under Zn-rich growth conditions with molecular NO and (or) NO₂ as the dopant source. This creates a shallow acceptor level via multi-site substitution of NO or NO₂ molecules, in such a way that one molecule occupies more than one normally O sites, which is energetically favored, and results in high hole concentrations. Another reason for the use of NO or NO₂ gas is that these gases further suppress the formation of donor-like defects such as oxygen vacancy (V_O) and metal interstitials (Zn_i), leading to high hole mobility. This unique concept of using molecules as dopants is the key to prevent the formation of other unwanted forms of molecules in the growth chamber and the formation of multi-site substitutional defects inside the material. In general, this molecular doping process can be used to grow various p-type transparent conducting oxides, such as ZnO, CdO, In₂O₃, SnO₂, Ga₂O₃ and the alloys thereof, with a molecular doping source, such that the oxide and doping source can be grown under conditions sufficient to deliver the doping source intact onto the oxide before it dissociates. This group has calculated the formation energy for the ZnO: N via substitution of atomic nitrogen as well as molecular NO or NO₂ in the O-sites of the ZnO matrix and showed that molecular substitution is energetically favored when NO or NO₂ molecule occupying more than one O-sites [205]. They also showed that the formation energies of N

related defects are largely reduced at the Zn-rich condition when NO or NO₂ gas is used as dopants, leading to significant enhancement of concentrations. The higher N chemical potentials (higher than $\frac{1}{2}\mu_{N_2}$) due to the NO or

NO₂ molecules are the reason for the defect formation energy reduction. The same principal can be applied to other transparent conducting oxide films too, which make the process more special. The schematic diagram of the NO / NO₂ incorporation inside ZnO matrix is illustrated in Fig. (12). As shown in the figure, Fig. (12-a) shows the structures of an NO and an NO₂ molecule. Fig. (12-b) shows the substitution of NO molecule in an O-site in such a way that the N-atom occupies a normal O-site of ZnO and, in effect, the O-atom of NO occupies an octahedral interstitial site (O_{oct}), denoted as (NO)_O-O. The O-atom of the NO molecule can also occupy a tetrahedral (T) interstitial site, which is denoted as (NO)_O-T (not shown here). This scheme is called single O-site substitution. On the other hand, when both the atoms of NO molecule occupy the normal O-site of ZnO matrix (denoted by (NO)_{OO}), the scheme is called double O-site substitution (as shown in Fig. (12-c)). For NO₂ molecular substitution, if the N-atom of the NO₂ molecule occupies a normal O-site of ZnO matrix, whereas the O-atoms of NO₂ molecule also occupy two other normal O-site, the scheme is called triple O-site substitution, as shown in Fig. (12-d).

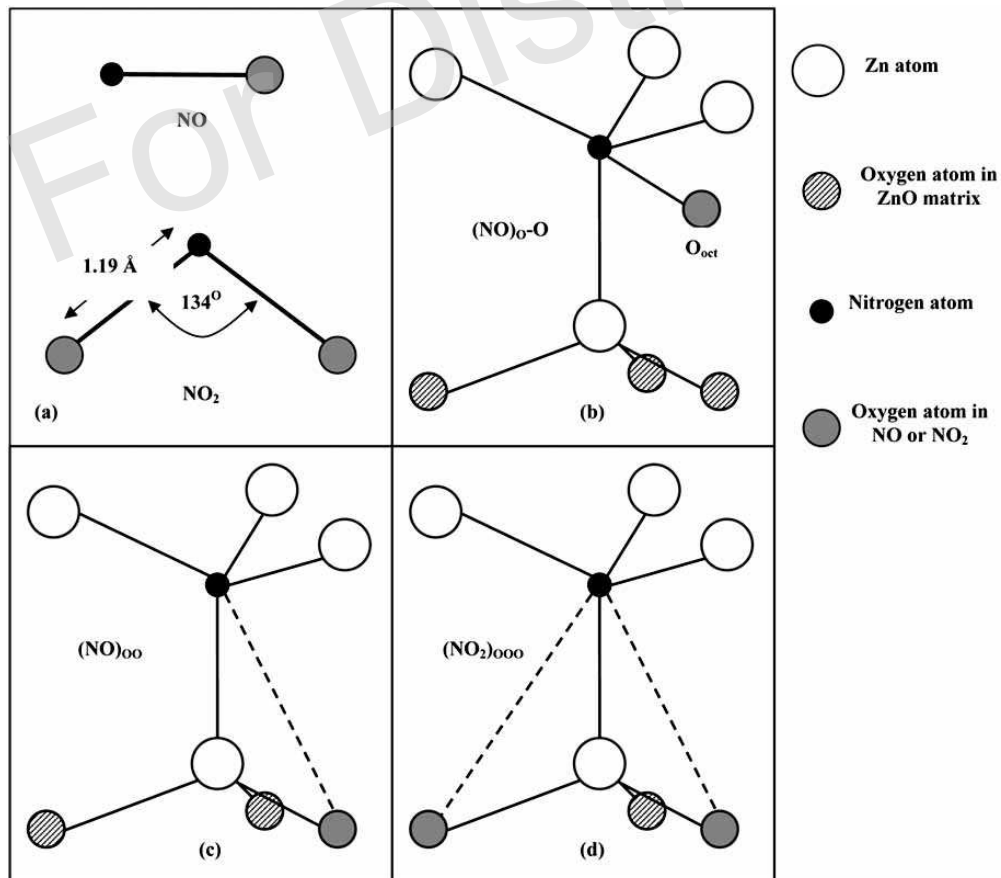


Fig. (12). Schematic illustration of the incorporation of NO and NO₂ molecule inside the ZnO matrix [205].

Similarly, Yoshida *et al.* [206] filed patent on the fabrication of p-type ZnO single crystal by a co-doping technique which comprises of p-type dopants such as nitrogen and carbon and an n-type dopant composed of any one or more elements selected from a group consisting of boron, aluminum, gallium, indium and hydrogen. The doping was done in such a way that the concentration of said p-type dopant is higher (between 1.5 to 5 times) than the concentration of said n-type dopant. When C is used as the p-type dopant, the material growth was done under Zn-rich condition. This is because C is a medium (not hard but not soft) basic element. When ZnO is doped with B, Al, Ga, or H, which are hard basic elements, as an n-type dopant together with such a C, since the chemical bonding of these elements with C is unstable, Zn is easily released. And a phenomenon occurs that C enters the vacancy produced after the Zn has been released. That is, C is in the state of easily substituting for Zn, a medium acid. This substitution means that C functions as an n-type dopant. Thereby, the crystallinity of ZnO doped with C together with B, Al, Ga, or H becomes unstable, and in the crystal, a phenomenon occurs in which C that functions as an n-type dopant offsets C that functions as a p-type dopant. Therefore, in the case of producing a p-type ZnO single crystal by this doping technology, it is preferable to supply zinc (Zn) excessively compared with oxygen (O). The chemical bonding occurs between Zn and C, which are both medium elements, and the substitution of Zn by C is prevented. As a result, since the crystallinity of ZnO doped with C together with B, Al, Ga, or H is stabilized and C functions only as a p-type dopant in this crystal. The p-ZnO single crystal containing p- and n-type dopants was grown on a semiconductor substrate by simultaneously supplying Zn, O, p-type dopants and n-type dopants using the MBE method. The said p- and n-type dopants are supplied in an atomic state produced by electrical excitation with radio waves, laser beams, X rays, electron beams etc. Fig. (13) shows the schematic structural diagram of a MBE growth chamber. The vacuum in the vacuum chamber is maintained at 10^{-8} torr and atomic gases

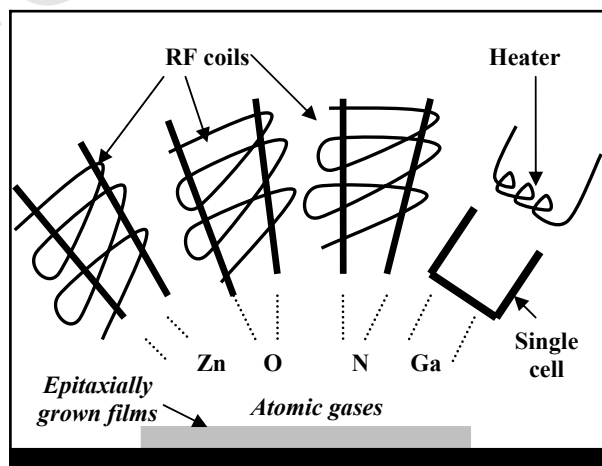


Fig. (13). MBE growth chamber of N-Ga co-doped p-ZnO film [206].

of Zn, O, N, and Ga etc. are supplied to the substrate through RF coils and heater. The hole conductivity in the single crystalline material is found to be around 10^{17} cm^{-3} .

Kakuya *et al.* [207] filed patent on the fabrication of co-doped p-ZnO: N-Ga via a two-step MBE growth technique. The schematic illustration of the process is shown in Fig. (14). In the first step atomic gases of Zn, O and p-type dopant (N) is supplied to grow ZnO on sapphire substrate. Thereafter, in the next step, the oxygen flow is stopped and a n-type dopant (Ga) is supplied to the system, thereby forming a p-type ZnO layer. By repeating these two steps, several numbers of times, a p-type ZnO based oxide semiconductor layer is grown. As a result, N to be the p-type dopant can be doped in a stable carrier concentration also during high temperature growth in which a residual carrier concentration can be reduced, and the carrier concentration of the p-type layer made of the ZnO based oxide semiconductor can be increased sufficiently.

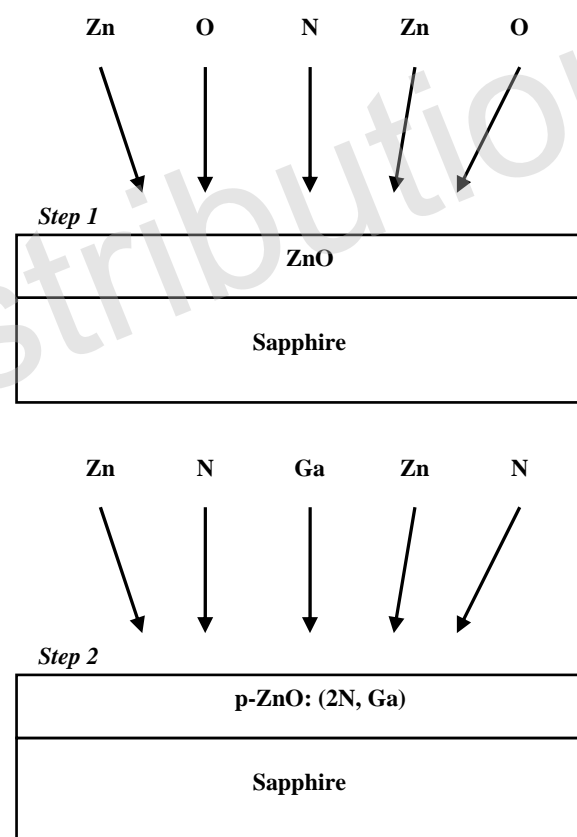


Fig. (14). Schematic diagram of N-Ga co-doped p-ZnO thin film [207].

As far as patenting activities on the transparent active devices, in the field of "Invisible Electronics", are concerned, White *et al.* [208] filed the patent for the fabrication of all-oxide transparent p-n homojunction diode of the form GaAs / p-ZnO: As / n-ZnO: Al by eximer pulsed laser deposition (PLD). A schematic diode structure is shown in Fig. (15-a). The current-voltage characteristic shows rectifying property with turn-on voltage around 1.0 V. In and Ga dopants were also used as the n-type donor atoms. Also GaN substrate is used for the fabrication of the junction instead of

GaAs. For GaAs substrate, a special substrate heat treatment is done so that As can migrate from the substrate to ZnO layer to make it p-type. But for GaN substrate, either As-doped ZnO pellet is directly used as the target for PLD or a molecular source of As is used during the growth, along with the ZnO target. In both cases, the acceptor atom concentration is set no less than 10^{15} cm^{-3} , so also the donor atom concentration is kept around 10^{15} cm^{-3} . Also they have fabricated transparent heterojunctions diode where the p-layer is made up of p-ZnO: As whereas the n-layer comprises of an oxide-based material whose bandgap is different from that of p-layer. This invention is important in the sense that the preparation of homoepitaxial and heteroepitaxial transparent p-n junctions can be accomplished using additional techniques in place of pulsed laser deposition such as MBE, MBE with laser ablation, CVD and MOCVD. Also, more complex devices such as transparent n-p-n, p-n-p transistors, FETs, photodetectors, lattice matching layers, and layers on which electrical leads may be attached can easily be fabricated using the above-described techniques and processes. Similarly, Kakuya and co-inventors [207] filed patent for the fabrication of a blue based (wavelength region from ultraviolet to yellow) p-n junction light emitting diode (LED) based on ZnO. The device structure is shown in Fig. (15-b), which is a double heterojunctions diode. All the layers are grown by MBE method on sapphire substrate. The fabrication technique described in this patent, in general, can be used to fabricate various oxide-based transparent homo- and (or) hetero-junction diode.

As far as nanostructured p-TCOs are concerned, Gong and co-authors [119] first reported the preparation of phase impure copper aluminum oxide thin films by chemical vapor deposition (CVD) method, which contain nanocrystalline phases of CuAlO_2 and Cu_2O . They have used metalorganic precursors $\text{Cu}(\text{acac})_2$ and $\text{Al}(\text{acac})_3$ ($\text{acac} = \text{acetylacetonate}$) as the source material. The crystallite size was found to be below 10 nm with an optical bandgap of 3.75 eV. The carrier concentration was $\sim 10^{19} \text{ cm}^{-3}$ [119]. Also later, Gao and co-authors [130] reported the synthesis of phase pure nanocrystalline CuAlO_2 thin film by spin-on technique. They have initially prepared CuAlO_2 nanocrystalline powder by hydrothermal cation exchange reaction between NaAlO_2 and CuCl . Then the powder was dispersed in alcohol and deposited as thin film on glass substrates by spin-on technique [130]. The average grain size obtained by this group was around 10 nm with an optical bandgap around 3.75 eV. The room temperature conductivity was found to be 2.4 S cm^{-1} with a hole concentration around 10^{18} cm^{-3} . We have also reported the synthesis of CuAlO_2 nanoparticles by D.C. sputtering technique from a sintered disk of copper aluminum oxide [209]. The particle size was found to be as low as 10 nm. We have observed an increase in the particle size with an increase in the deposition time. Also an increase in the bandgap from 3.60 to 3.94 was observed with the decrease in the particle size. And this bandgap enhancement is attributed to the quantum confinement effect as often found in semiconductor nanocrystals. We have also observed, for the first time some photoluminescence properties of nanocrystalline CuAlO_2 thin films and tried to explain it with existing theories [209]. Photoluminescence properties of p-

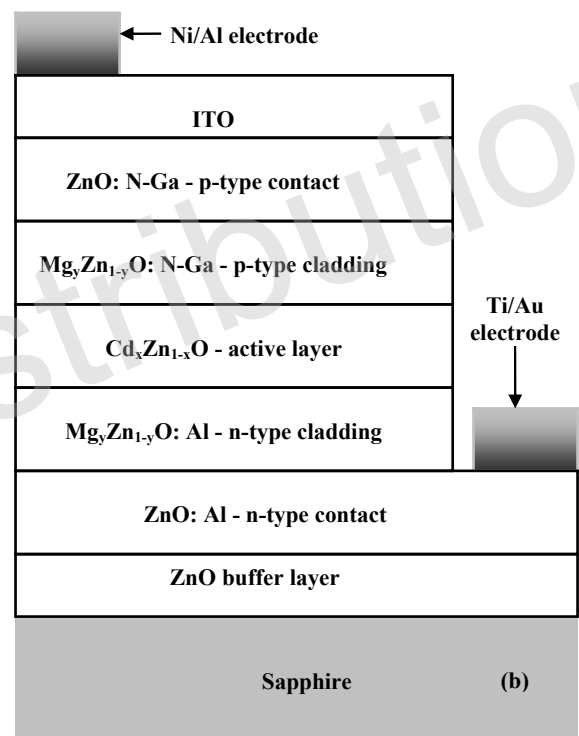
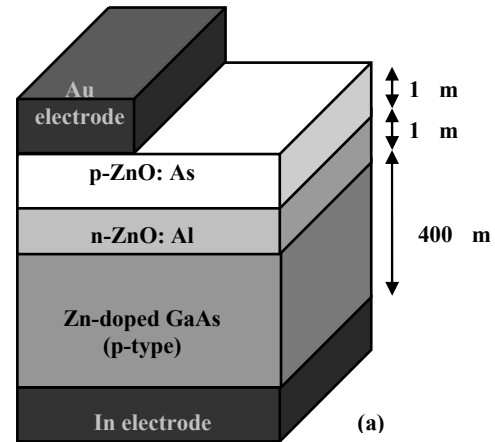


Fig. (15). Schematic structure of ZnO-based (a) transparent p-n homojunction [208] (b) LED [207].

type transparent semiconducting layered oxysulphide thin films of $\text{LaO}(\text{CuS})$ have been reported previously by Ueda and co-authors [80]. Also, as far as luminescence properties of copper based delafossite oxide materials are concerned, Jacob and co-authors [210] reported the luminescence properties of CuLaO_2 and CuYO_2 pellets. Various optoelectronic properties of nanocrystalline CuAlO_2 thin film are furnished in Table 10. As far as non-delafossite p-TCO nanostructure is concerned, recently, Xiang *et al.* [211] reported the fabrication of highly oriented p-ZnO: P nanowires by simple chemical vapor deposition method. The p-type dopant source is taken as P_2O_5 and well-aligned single-crystalline nanowires are grown on the sapphire substrate. The average diameter and length of the nanowires are 50 nm and 2 μm respectively.

Table 10. Electro-Optical Properties of Nanostructured CuAlO₂ Thin Films Synthesized by Various Processes

Process	Avg. Particle Size (nm)	Band-Gap (eV)	Room-Temp. Conductivity (S cm ⁻¹)	Carrier Concentration (cm ⁻³)	Ref	Remarks
MO-CVD	10	3.75	2.0	1.8 x 10 ¹⁹	119	The film contains nanocrystalline phases of CuAlO ₂ and Cu ₂ O.
Spin-on technique	10	3.75	2.4	5.4 x 10 ¹⁸	130	Initially CuAlO ₂ nanocrystalline powder was prepared by hydrothermal cation exchange reaction between NaAlO ₂ and CuCl. Then the powder was dispersed in alcohol and deposited as thin film.
Sputtering	~10	3.94	---	---	209	Deposition time was varied to decrease the particle size. With decrease in the particle size, an increase in the bandgap is observed due to quantum confinement effect. Also room-temp. photoluminescence properties were observed first time in these nanocrystalline CuAlO ₂ thin films.

4. FABRICATION OF p-CuAlO₂ NANO-PARTICLES BY LOW-COST D.C. SPUTTERING TECHNIQUE

Nanostructured p-CuAlO₂ thin films have been synthesized by D.C. sputtering technique by reducing the deposition time and substrate temperature during deposition. Effect of deposition time on crystal quality, particle size, strain, bandgap etc of the film has been investigated. Also photoluminescence properties of this nanocrystalline material have been reported here.

4.1. Fabrication

Polycrystalline CuAlO₂ powder was first synthesized by mixing Cu₂O and Al₂O₃ powders (both 99.99 %) with Cu / Al atomic ratio 1 : 1 for 1 hr. Then the mixture was then air-annealed at 1100°C for 24 hours to form the CuAlO₂ powder. The sintered body was then reground and pressed into pellet by hydrostatic pressure and was placed in aluminum holder by some appropriate arrangement, which was used as the target for sputtering.

The sputtering unit was evacuated by standard rotary-diffusion arrangement upto a base pressure of 10⁻⁶ mbar and the target was then pre-sputtered for 10 min to remove contamination, if any, from the surface and then the shutter was displaced to expose the substrates in the sputtering plasma. Films were deposited on ultrasonically cleaned glass and Si substrates, which were placed on the lower electrode and connected to the ground of the power supply. The electrode distance was taken as 1.5 cm. Ar and O₂ (3 : 2 vol. ratio) were taken as sputtering gases. Details of the deposition conditions were described elsewhere [209]. Most importantly, the deposition times (t_d) of the films were kept at very low values, which range from 3 min to 45 min and also the substrate temperature was kept at ambient condition (373 K). This is because, generally at higher substrate temperature, the particles tend to coalesce to form bigger clusters, which is unwanted for the formation of nano-structured films. The variation in the deposition time is done to observe the changes in the nanostructure and optical

properties of the films. Also no post-annealing of the films was performed.

4.2. Characterization

The X-ray diffraction pattern of the synthesized CuAlO₂ powder, which was used for target preparation, has been presented in Fig. (16-a). The peaks of the powdered material confirm the proper phase formation of the required target material. Fig. (16-b) and (16-c) represent the XRD patterns of sputter-deposited nanocrystalline CuAlO₂ thin films on Si substrates with deposition times (t_d) 45 min and 15 min respectively. For the film with t_d = 15 min, two broad peaks of (101) and (012) reflections are observed along with two smaller peaks of (107) and (018) reflections. On the other hand for the film deposited in 45 min, a slightly stronger peak of (006) reflections and a small peak of (018) reflections are observed along with the presence of a broad and considerably attenuated hump representing (101) and (012) reflections.

Transmission electron microscopic (TEM) analyses were done for nanocrystalline CuAlO₂ thin films with various deposition times (t_d). Fig. (17-a), (17-b) and (17-c) show the TEM micrographs of CuAlO₂ films deposited in 3, 9 and 15 min respectively. From the micrographs, the average particle sizes (L) are obtained around 10 nm, 20 nm and 30 nm respectively, for the films deposited in 3 min, 9 min and 15 min respectively. Previously, Gong *et al* [119] and Gao *et al* [130] reported the particle size of their nanocrystalline copper aluminum oxide films around 10 nm, which is comparable to our samples deposited in 3 min. Also, from the TEM micrographs we have observed an increase in the average particle size of our nanocrystalline CuAlO₂ thin films with increase in the deposition times, which is mainly due to the greater amount of influx of sputtered particles, resulting into the agglomeration of bigger particles. Thus the average particle size increases with increase in the deposition time as observed in Fig. (17-a), (17-b) and (17-c) and when the deposition time is 45 min and above, the average particle size (L) becomes ~ 60 nm and more (not shown here).

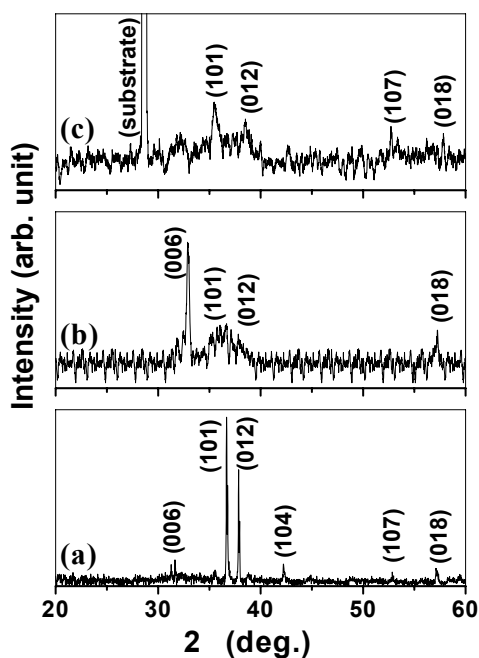


Fig. (16). XRD pattern of (a) p-CuAlO₂ sintered target, (b) nanocrystalline p-CuAlO₂ thin film deposited for 45 min., (c) for 15 min.

Selected area electron diffraction pattern (SAED) of the films deposited in 3 min, 9 min and 15 min are shown in the Fig. (17-d), (17-e) and (17-f). Few diffraction rings are obtained in all the patterns which correspond to the (101) & (202) planes of the films deposited in 3 min, (101) & (0012) for the films with $t_d = 9$ min and (101) & (018) for the films deposited in 15 min respectively. The lattice spacings (d) corresponding to these rings in the diffraction patterns were measured with the camera constant of the

equipment and the diffraction ring radii were measured from the micrographs [212]. These 'd'-values calculated from all the patterns along with that obtained from XRD measurements were then matched with the theoretical 'd'-values obtained from JCPDS file [213] and compared in Table 11.

It has been observed that in all the SAED patterns, a (101) orientation is present, which is similar to the target material as well as to that of the film deposited for 15 min (as shown in the XRD pattern). Therefore, this observation basically indicates the formation of quasi-continuous films consisting of CuAlO₂ nano-particles, when the deposition time is 15 min or less, (as has been depicted from TEM micrographs), whereas with further increase in the deposition time (i.e. for $t_d \geq 45$ min), the growth mechanism followed a preferred (006) orientation.

UV-Vis spectrophotometric measurements of CuAlO₂ thin films were done for the samples with deposition times 3 min, 9 min, 15 min, 45 min and 150 min. Fig. (18-a) shows the spectral variation of the transmittance (T) of these films deposited on glass substrates taking similar glass as reference. Therefore the spectra are for the films only. Thickness of the films are in the range of 30 nm, 60 nm, 90 nm, 200 nm and 400 nm for the films deposited in 3 min, 9 min, 15 min, 45 min and 150 min respectively. The average visible transmittance of these films increases from 75% to 98% with decrease in the deposition time. This is mainly due to the decrease in the film thickness, which leads to lesser scattering and absorption of photons. Fig. (18-b) represents the spectral variation of reflectance (R) of the same films deposited on glass substrates. From the transmittance (T) and reflectance (R) data, the absorption coefficients (α) of these films were measured according to the following equation

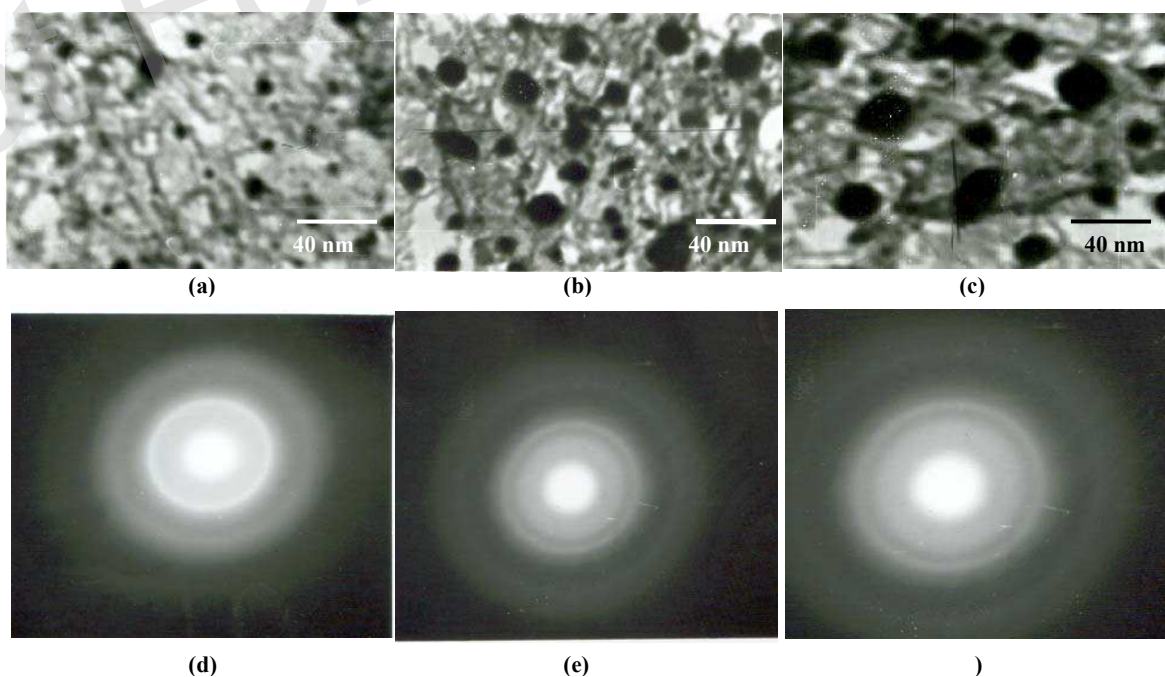


Fig. (17). TEM micrographs of p-CuAlO₂ nanoparticles deposited for (a) 3 min., (b) 9 min. and (c) 15 min. (d) SAED pattern of the same for deposition time 3 min (e) 9 min. and (f) 15 min.

Table 11. Comparison Between the Experimentally Obtained d-Values from SAED Patterns (d_{SAED}) of the Nano-Crystalline p-CuAlO₂ Thin Films Deposited for 3 min and 9 min and that of XRD Patterns (d_{XRD}) for the Target and Films Deposited for 15 min and 45 min Respectively with that given in JCPDS File (d_{JCPDS})

h k l	d_{SAED} (Å)			d_{XRD} (Å)			d_{JCPDS} (Å)
	$t_d = 3$ min	$t_d = 9$ min	$t_d = 15$ min	$t_d = 15$ min	$t_d = 45$ min	Target	
0 0 6	---	---	---	---	2.816	2.83	2.820
1 0 1	2.438	2.441	2.450	2.448	2.450	2.45	2.437
0 1 2	---	---	---	2.350	2.380	2.378	2.376
104	---	---	---	---	---	2.133	---
1 0 7	---	---	---	1.732	---	1.732	1.732
0 1 8	---	---	1.618	1.607	1.610	1.611	1.612
0 0 2	---	1.406	---	---	---	1.401	1.401
2 0 2	1.220	---	---	---	---	1.225	1.225

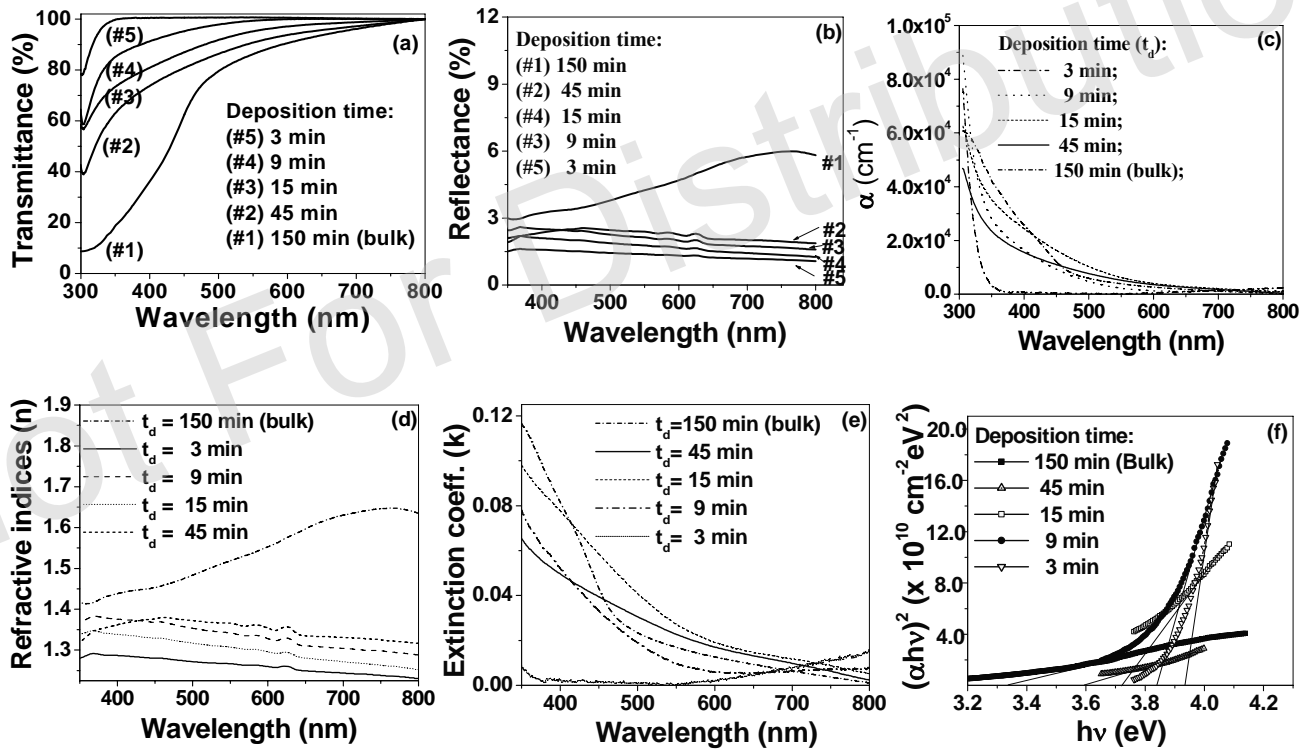


Fig. (18). Spectral variation of the (a) transmittance, (b) reflectance, (c) absorption coefficient, (d) refractive index, (e) extinction coefficient and (f) bandgap determination of p-CuAlO₂ nano-particles.

$$\alpha = \frac{1}{d} \ln \left[\frac{1-R}{T} \right] \quad (3)$$

where T is the transmittance, R is the reflectance, α is absorption coefficient and d is the thickness of the film (here, we have neglect the internal multiple reflections, as the film thickness is very low). (Fig. 18-c) represents the spectral variation of α in the visible range. The value of α varies from $8.61 \times 10^2 \text{ cm}^{-1}$ for film deposited for 3 min to

$2.56 \times 10^4 \text{ cm}^{-1}$ for film deposited for 150 min (bulk film) at 400 nm wavelength. Also the refractive indices (n) and extinction coefficients (k) of these films were determined according to Eq. 4 and Eq. 5 respectively using the values of α and R . Fig. (18-d) and (18-e) show the wavelength (λ) vs. n and k plots respectively.

$$n = \frac{1 + \sqrt{R}}{1 - \sqrt{R}} \quad (4)$$

and

$$k = \frac{\lambda \alpha}{4\pi} \quad (5)$$

Here, for transparent medium (as for p-CuAlO₂ films), we have assumed that $k^2 \ll (n-1)^2$.

In the range of the onset of absorption edge, the absorption coefficients can be described by the relation for parabolic bands according to the following equation

$$(\alpha h\nu)^{1/n} = A(h\nu - E_g) \quad (6)$$

where E_g is the band gap of the material and the exponent n depends on the type of transition. For direct allowed transition, $n=1/2$, for indirect allowed transition, $n=2$, and for direct forbidden transition, $n=3/2$. The factor A is a constant but also depends on the type of transition. The $(\alpha h\nu)^2$ vs.

$h\nu$ plots for the films with different deposition times (t_d) is shown in Fig. (18-f). The direct allowed bandgap values for the films deposited for 3 min, 9 min, 15 min, 45 min and 150 min are obtained as 3.94 eV, 3.84 eV, 3.72 eV, 3.60 eV and 3.34 eV respectively. The corresponding average particle sizes (L) are 10 nm, 20 nm, 30 nm, 60 nm and greater than 90 nm respectively. Various optical parameters of nanocrystalline CuAlO₂ films deposited for different times are compared in Table 12. From the table, we have observed the broadening of the bandgap energy of our nanocrystalline CuAlO₂ thin film with the decrease in the deposition time. This may be attributed to the quantum confinement effect put forward by Brus [157] where the size dependency of the bandgap of a semiconductor nanoparticle ($E_{g[nano]}$) is

given by the following formula:

$$\Delta E = E_{g[nano]} - E_{g[bulk]} = \frac{h^2}{8\mu^* (\frac{L}{2})^2} - \frac{1.8e^2}{(\frac{L}{2})\epsilon} \quad (7)$$

where ΔE is the shift of the bandgap with respect to the bulk bandgap $E_{g[bulk]}$, $\frac{L}{2}$ is the radius of the nano-particles

(where L is the particle diameter, taken to be equivalent to the particle size, mentioned earlier), μ^* is the reduced mass of electron-hole effective masses and ϵ is the semiconductor dielectric constant. The first term of the RHS expression in the equation represents the particle-in-a box quantum localization energy and has a $\frac{1}{L^2}$ dependence for both electron and hole. The 2nd term represents the Coulomb energy with an $\frac{1}{L}$ dependence. In the limit of large L , the value of $E_{g[nano]}$ approaches that of $E_{g[bulk]}$. As TEM micrographs (Fig. (17-a), 17-b and 17-c)) reveal that the average particle size of our samples decreases with the decrease in the deposition time (i.e. $L \sim 10$ nm and ~ 20 nm for $t_d = 3$ min & 9 min respectively and for $t_d = 15$ min and 45 min, $L \sim 30$ nm and ~ 60 nm), the observation of bandgap widening in our samples is consistent with the quantum confinement effect explained by the Eq. 6.

The size-dependant optical properties of CuAlO₂ nanoparticles were examined by the photoluminescence (PL) spectroscopic measurements at room temperature. The PL spectra shown in Fig. (19) were obtained with a 210 nm excitation wavelength and the films were deposited on Si substrates. Three spectra shown in the Fig. (19) are for three samples deposited for 9 min (curve - a), 15 min (curve - b) and 45 min (curve - c) respectively. Three peaks obtained are around 3.56 eV, for curve - c ($\lambda = 348.5$ nm), 3.61 eV, for curve - b ($\lambda = 343.6$ nm) and 3.66 eV, for curve - a ($\lambda = 339.0$ nm) respectively. These peaks may be attributed to the UV near-band edge (NBE) emission [214] of wide bandgap CuAlO₂, namely the recombination of free excitons through an exciton-exciton collision process. This observation again indicates the existence of direct transition type bandgap of this material, which is favorable for the optoelectronics applications like light-emitting diodes (LED). Also, a slight blue-shift of the emission peaks is observed with decrease in the deposition time. As already mentioned previously, that a decrease in the average particle size (L) is observed with the decrease in the deposition time, t_d (i.e. for $t_d = 9$ min, 15 min and 45 min, $L \sim 20$ nm, ~ 30 nm and ~ 60 nm respectively),

Table 12. Variation of Average Particle Size, Film Thickness and Bandgap with the Deposition Time of Nano-Crystalline CuAlO₂ Thin Film

t_d (min)	Average particle size (nm)	Film thickness (nm)	Avg. T (%)	α (at $\lambda=400$ nm) (cm ⁻¹)	n (at $\lambda=400$ nm)	k (at $\lambda=400$ nm)	Band-gap (eV)
3	~ 10	30	95	8.61×10^2	1.29	0.003	3.94
9	~ 20	60	90	1.63×10^4	1.38	0.05	3.84
15	~ 30	90	80	2.44×10^4	1.34	0.08	3.72
45	~ 60	200	75	1.56×10^4	1.36	0.05	3.60
150 (bulk)	> 90	400	65	2.56×10^4	1.44	0.08	3.34

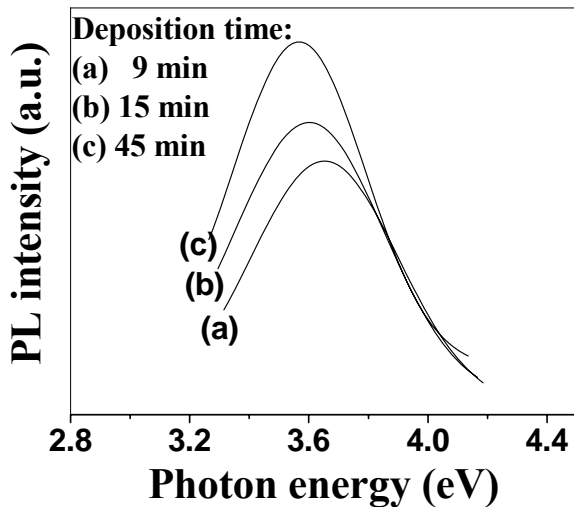


Fig. (19). Photoluminescence spectra (PL) spectra of nano-structured CuAlO_2 thin films deposited for (a) 9 min, (b) 15 min and (c) 45 min.

therefore this blue-shift may be another indication of experimentally observed bandgap enhancement results from low-dimensional quantum confinement effects.

Hall measurements could not be performed in all of our samples. But p-type conductivity of the sample deposited for 150 min was established by thermo-power measurement and the positive value of room temperature Seebeck coefficient ($S_{RT} = +93 \mu\text{V K}^{-1}$) of this sample confirmed the p-type nature of the film. But for the films deposited for 45 min and less, thermo-power measurement could not be performed and only hot-probe measurements confirmed the p-type conductivity in these films.

In conclusion, it has been observed that the nano-structured p-type conducting CuAlO_2 thin films, synthesized by D. C. sputtering technique, showed a variation in the particle size with a variation in the deposition time. Optical transmission spectra of the films also show an increase in the average visible transmittance with decrease in deposition time. A blue-shift and widening of the bandgap of the material is observed with decrease in deposition time. As particle size decreases with decrease in the deposition time, this bandgap broadening is attributed to the quantum confinement effect, where the bandgap of a semiconductor nanoparticle becomes an inverse function of the particle size. Room temperature photoluminescence measurements of this material showed UV bands around 3.56 eV to 3.66 eV for the films deposited for 45 min to 9 min respectively, which arises from the room temperature excitons. The existence of room-temperature excitons in CuAlO_2 is supposed to originate from low relative dielectric constant of the material and high reduced mass of the excitons, which produces large exciton binding energy. A blue-shift of the emission peaks is observed with decrease in the particle size, confirming the quantum confinement effect within the CuAlO_2 nanoparticles. Therefore, fabrication of nano-structured p- CuAlO_2 and other types of p-TCOs, coupled with the already existing and well-known materials of nano-structured n-TCOs, will give an added impetus in the field of "Invisible Electronics" for the fabrica-

tion of nano-active devices, which can have high-efficient applications in the optoelectronics device technology.

5. CURRENT & FUTURE DEVELOPMENTS

Currently, a major part of the research activities in p-TCO technology are concentrated on the fabrication of device quality films with superior electrical characteristics. The maximum conductivity of p-TCO films reported so far is still few orders of magnitude less than that of commercially available n-TCO films. So this puts hindrance in the formation of effective active devices for large-scale production. It is found that nonstoichiometric oxygen intercalation within the material has its limitation to increase the conductivity of the film. Excess oxygen intercalation, beyond an optimum value, is found to deteriorate the film quality [107]. So intentional doping of the material is the obvious step to increase the conductivity of the film. Identification of proper dopant and doping procedure should be the focus of the future work in this field. Several theoretical articles have been published so far [180-181, 215-217], indicating various doping materials and procedures to enhance the electrical characteristics of these materials but no experimental work has yet been reported, as far as literature survey goes. Therefore, doping of p-TCOs for superior device quality films is an important area of research for the development of "Transparent Electronics". In this regard, another important direction should be mentioned here is the development of various new kinds of p-TCOs, having diverse characteristics. Recently, new types of p-TCOs in the form of spinel ZnM_2O_4 (M: Co, Ir, Rh) [218,219] and SnO_2 : M (M: In, Ga) [220,221] have been reported, which show considerably high conductivity. These results may lead to different new kinds of p-TCOs with superior electro-optical properties.

Another interesting area of research is the cost-effective fabrication of transparent junctions, without compromising its electro-optical properties. This is important for the large-scale production of various junctional devices for diverse applications in "Transparent Electronics". Costly techniques like PLD [222] may produce superior junctions, but for large-scale production, cost-effective techniques are the needs of the hour [144, 187, 223]. It is noteworthy that the ZnO-based LEDs are recently gained renewed interest in optoelectronics technology [188] for potential applications in short-wavelength LEDs and diode lasers in the field of display, illumination and information storage technology. Therefore, this field has tremendous potential to explore high-efficient devices.

Another area of research, which is not yet explored completely, but has tremendous potential, is the thermoelectric properties of CuAlO_2 films. Being a layered-structured material, this material as well as other delafossite materials (so also other superlattice materials) can become very good candidate for thermoelectric converters. Recently, Park *et al* [224] have reported a significant increase in the thermoelectric properties of this material for Ca substitution in Al sites at high temperature. They have observed the highest value of power factor around $7.82 \times 10^{-5} \text{ Wm}^{-1} \text{ K}^{-2}$ for $\text{CuAl}_{0.9}\text{Ca}_{0.1}\text{O}_2$ at 1140 K. Also, recently, Hicks and co-authors [225-227] theoretically showed that low-dimensional

materials (such as quantum wires, quantum dots of different thermoelectric materials) can have superior thermoelectric properties over the corresponding bulk materials. This is assumed to be due to the confinement of the electrons and phonons inside the low-dimensional environment of the nanostructures, which manifests the superior Figure-of-merit ($ZT = \frac{S^2\sigma T}{\kappa}$, also called dimensionless Figure-of-merit,

where S is the Seebeck Coefficient, σ is the electrical conductivity, κ is the thermal conductivity and T is the temperature [228]) of these nanomaterials. Therefore, nanostructured p-CuAlO₂ and similar p-TCOs may provide new and high-efficient thermoelectric materials and, hence, if proper studies can be done on the thermoelectric properties of these types of superlattice and nanostructured materials, new horizon may open up in the field of thermoelectric converters.

Also keeping an eye in the tremendous progress in nanotechnology, fabrication and characterization of nanostructured p-CuAlO₂ as well as other p-TCO thin films may become an important field of work, because of new and interesting properties exhibited by these nano-materials [209, 211]. Proper fabrication procedure to get reproducible nano-materials is the most important future work. Also in-depth studies of the photoluminescence properties of p-CuAlO₂ and similar types of p-TCO nano-particles will be another area of research, which is needed to be explored properly. Fabrication of nano-structured p-TCOs, coupled with the already existing and well-known materials of nano-structured n-TCOs, will give an added impetus in the field of "Invisible Electronics" for the fabrication of nano-active devices, which can have high-efficient applications in the optoelectronics device technology.

Field-emission property of CuAlO₂ thin films is a completely new area of research, which has tremendous opportunities [229,230]. This material showed very low turn-on field comparable to most of the carbonaceous low-threshold field-emitters like carbon nanotube (CNT), diamond like carbon (DLC), diamond, amorphous carbon (a:C), silicon carbide (SiC) nanorods etc. So these types of p-TCO materials may become promising alternative to the existing materials in the field of FED technology. But, proper emission mechanism in these materials is not very clear till date and very good scopes are there to properly investigate the emission mechanism so that the material properties can be tuned accordingly to get better field-emission properties of these films.

Also recent study showed that p-CuAlO₂ can become a good candidate for ozone sensors. Zheng and co-authors [231] reported that CuAlO₂ has a selective and reversible response to ozone gas at room temperature. All existing commercial semiconductor ozone sensors are of n-type [232-235]. This study demonstrated the feasibility of developing an inexpensive p-type transparent ozone sensor. Hence, transparent p-n junction ozone sensors may be fabricated using the p-CuAlO₂ and existing n-TCO such as In₂O₃.

Photocatalytic hydrogen evolution over delafossite CuAlO₂ is another interesting report published recently by Koriche *et al.* [236]. This group proposed a new photoche-

mical system for water reduction based on p-CuAlO₂ and S²⁻ as hole scavenger. They have used co-precipitation method, a new synthetic route, to synthesis CuAlO₂, which increased the surface to volume ratio and delivered a highest H₂ production. This report is very interesting and shows newer applications of delafossite p-CuAlO₂ and similar p-TCO materials.

Also, recently Kizaki and co-authors [237] proposed a material-designing procedure to get CuAlO₂-based dilute magnetic semiconductors. Ab-initio calculations showed that Fe- and Mn-doped CuAlO₂-based dilute magnetic semiconductors possess high-Curie-temperature ferromagnetic characteristics. Being a natural p-type transparent semiconductor without intentional doping, CuAlO₂ can easily be used for the host of dilute magnetic semiconductors. Also, most importantly, the delafossite structure of CuAlO₂ has the advantage of possessing two cation-sites, Cu⁺¹ and Al⁺³ sites, for possible magnetic ion substitution. O-Cu-O dumbbell-sites in delafossite CuAlO₂ can be partially replaced with magnetic ions. Due to this coordination one can realize new ferromagnetic dilute magnetic semiconductors from the standpoint of the hybridization of orbitals between 3d orbitals with the impurities and 2p orbitals with the oxygen in CuAlO₂. Similarly, Diet *et al.* [201] recently showed that Mn-doped p-type ZnO can become a good candidate for magnetic semiconductors having potential application in spintronics.

Therefore, it will not be an exaggeration to say that next decade will see the renaissance of micro/nano-structured p-TCO materials and various new, interesting and novel technological applications with these materials are on the verge of exploration.

ACKNOWLEDGEMENT

The authors wish to gratefully acknowledge the financial assistance of the Department of Science and Technology, Govt. of India, during the execution of the work.

REFERENCES

- [1] Badekar K. (Leipzig) Ann Phys 1907; 22: 749.
- [2] Lampert CM. Heat mirror coatings for energy conserving windows. Sol Energy Mater 1981; 6: 1-41.
- [3] Chopra KL, Major S, Pandya DK. Transparent conductors. A status review. Thin Solid Films 1983; 102: 1-46.
- [4] Hamberg I, Granqvist CG. Evaporated Sn-doped In₂O₃ films: basic optical properties and applications to energy-efficient windows. J Appl Phys 1986; 60: R123-R160.
- [5] Holland L. Vacuum Deposition of Thin Films, Wiley. New York. 1958; 492-495.
- [6] Cachet H, Gamard A, Campet G, Jousseume B, Toupance T. Tin dioxide thin films prepared from a new alkoxyfluorotin complex including a covalent Sn---F bond. Thin Solid Films 2001; 388: 41-49.
- [7] Wendt R, Ellmer K. Desorption of Zn from a growing ZnO:Al-film deposited by magnetron sputtering. Surf. Coat Technol 1997; 93: 27-31.
- [8] Hartnagel HL, Dawar AL, Jain AK, Jagadish C. Semiconducting transparent thin films. IOP Publishing Ltd. Bristol and Philadelphia 1995.
- [9] Ginley DS, Bright C. Transparent conducting oxides. MRS Bulletin 2000; p.15.
- [10] Cava RJ, Philips JM, Kwo J, *et al.* GaInO₃: A new transparent conducting oxide. Appl Phys Lett 1994; 64: 2071-2072.
- [11] Philips JM, Cava RJ, Thomas GA, *et al.* Zinc-indium-oxide: A high conductivity transparent conducting oxide. Appl Phys Lett 1995; 67: 2246-2248.

- [12] Freeman AJ, Poeppelmeier KR, Mason TO, Chang RPH, Marks TJ. Chemical and thin-film strategies for new transparent conducting oxides. *MRS Bulletin* 2000; p.45.
- [13] Gordon RG. Criteria for choosing transparent conductors. *MRS Bulletin* 2000; p.52.
- [14] Mochel, J. M.: US2564706 (1947).
- [15] Sinclair WR, Peters FG, Stillinger DW, Koonce SE. Devitrification of tin oxide films (doped and undoped) prepared by reactive sputtering. *J Electrochem Soc* 1965; 112: 1096-1100.
- [16] Lytle, W. O., Junge, A. E.: US2566346 (1951).
- [17] Gordon, R. G.: US4146657 (1979).
- [18] Banerjee AN, Kundoo S, Saha P, Chattopadhyay KK. Synthesis and characterization of nano-crystalline fluorine-doped tin oxide thin films by sol-gel method. *J Sol-Gel Sci Technol* 2003; 28: 105-110.
- [19] Banerjee AN, Maity R, Kundoo S, Chattopadhyay KK. Poole - Frenkel effect in nanocrystalline SnO₂: F thin films prepared by sol-gel-dip-coating technique. *Phys Stat Solidi A* 2004; 201: 983-989.
- [20] Major S, Banerjee A, Chopra KL. Annealing studies of undoped and indium-doped films of zinc oxide. *Thin Solid Films* 1984; 122: 31-43.
- [21] Minami T, Nanto H, Takata S. Highly conductive and transparent aluminum doped zinc oxide thin films prepared by RF magnetron sputtering. *Jpn J Appl Phys Part 2 Lett* 1984; 23: L280-L282.
- [22] Hu J, Gordon RG. Textured fluorine-doped ZnO films by atmospheric pressure chemical vapor deposition and their use in amorphous silicon solar cells. *Sol Cells* 1991; 30: 437-450.
- [23] Vijayakumar, P.S., Blaker, K.A., Welting, R.D., Wong, B., Halani, A. T., Park, C.: US4751149 (1988).
- [24] Choi BH, Im HB, Song JS, Yoon KH. Optical and electrical properties of Ga₂O₃-doped ZnO films prepared by r.f. sputtering. *Thin Solid Films* 1990; 193: 712-720.
- [25] Hu J, Gordon RG. Atmospheric pressure chemical vapor deposition of gallium doped zinc oxide thin films from diethyl zinc, water, and triethyl gallium. *J Appl Phys* 1992; 72: 5381-5392.
- [26] Mochel, J. M.: US2564707 (1951).
- [27] Holland L, Siddall G. *Vacuum*, Springer Vol. III, 1955.
- [28] Avaritsiotis JN, Howson RP. Composition and conductivity of fluorine-doped conducting indium oxide films prepared by reactive ion plating. *Thin Solid Films* 1981; 77: 351-357.
- [29] Groth R. Untersuchungen an halbleitenden Indiumoxydschichten. *Phys Stat Solidi* 1966; 14: 69-75.
- [30] Nozik, A. J.: US3811953 (1974).
- [31] Haacke G, Mealmaker WE, Siegel LA. Sputter deposition and characterization of Cd₂SnO₄ films. *Thin Solid Films* 1978; 55: 67-81.
- [32] Vossen JL. *RCA Rev* 1971; 32: 269-271.
- [33] Enoki H, Nakayama T, Echigoya J. The electrical and optical properties of the ZnO-SnO₂ thin films prepared by RF magnetron sputtering. *Phys Stat Solidi A* 1992; 129: 181-191.
- [34] Minami T, Sonohara H, Takata S, Sato H. Highly transparent and conductive zinc-stannate thin films prepared by RF magnetron sputtering. *Jpn J Appl Phys Part 2 Lett* 1994; 33: L1693-L1696.
- [35] Cava RJ, Hou SY, Krajewski JJ, *et al.* Transparent conducting thin films of GaInO₃. *Appl Phys Lett* 1994; 65: 115-117.
- [36] Otabe T, Ueda K, Kudoh A, Hosono H, Kawazoe H. *n*-type electrical conduction in transparent thin films of delafossite-type AgInO₂. *Appl Phys Lett* 1998; 72: 1036-1038.
- [37] Dali SE, Jayachandran M, Chockalingam MJ. New transparent electronic conductor, MgIn₂O₄ spinel. *J Mater Sc Lett* 1999; 18: 915-917.
- [38] Edwards DD, Mason TO, Goutenoire F, Poeppelmeier KR. A new transparent conducting oxide in the Ga₂O₃-In₂O₃-SnO₂ system. *Appl Phys Lett* 1997; 70: 1706-1708.
- [39] Minami T, Takata S, Kakumu T, Sonohara H. New transparent conducting MgIn₂O₄-Zn₂In₂O₅ thin films prepared by magnetron sputtering. *Thin Solid Films* 1995; 270: 22-26.
- [40] Minami T, Kakumu T, Shimokawa K, Takata S. New transparent conducting ZnO-In₂O₃-SnO₂ thin films prepared by magnetron sputtering. *Thin Solid Films* 1998; 317: 318-321.
- [41] Omata T, Ueda N, Ueda K, Kawazoe H. New ultraviolet-transport electroconductive oxide, ZnGa₂O₄ spinel. *Appl Phys Lett* 1994; 64: 1077-1078.
- [42] Kammler DR, Mason TO, Young DL, Coutts TJ. Thin films of the spinel Cd_{1-x}In_{2-2x}Sn_{2x}O₄ transparent conducting oxide solution. *J Appl Phys* 2001; 90: 3263-3268.
- [43] Minami T. New *n*-Type Transparent Conducting Oxides. *MRS Bull* 2000; p.38.
- [44] Lewis BG, Paine DC. Applications and processing of transparent conducting oxides. *MRS Bull* 2000; p. 22.
- [45] Granqvist CG, Azens A, Hjelm A, *et al.* Recent advances in electrochromics for smart windows applications. *Sol. Energy* 1998; 63: 199.
- [46] Kammler DR, Edwards DD, Ingram BJ, *et al.* Photovoltaics for the 21st Century, edited by Kapur VK, McConnel RD, Carlson D, Ceasan GP, Rohatgi A. The Electrochem Soc Proc 99-11, Pennington NJ 1999; p. 68.
- [47] Lee SH, Hwang KH, Joo SK. In electrochromic materials (2nd International Symposium), edited by Ho KC, McArthur DA. The Electrochem Soc Proc 94-2 Pennington NJ 1994; p. 290.
- [48] Lugg PS, Bommarito S, Bailey J, *et al.* Solid State Ionic Devices. The Electrochem Soc Proc 99-13 Pennington NJ 1999; p. 284.
- [49] Nakato Y, Kai KI, Kawabe K. Improvement of characteristics of new-type solar cells, having a "transparent conductor/thin SiO₂ layer with ultrafine metal particles as conductive channels/n-Si" junction. *Sol Energy Mater Sol Cells* 1995; 37: 323-335.
- [50] Emons TT, Li J, Nazar LF. Synthesis and characterization of mesoporous indium tin oxide possessing an electronically conductive framework. *J Am Chem Soc* 2002; 124: 8516-8517.
- [51] Hutchins, M.G., McMeeking, G.D.: Biosensor Patent No. 9027607.2 (1990).
- [52] He Y, Kanicki J. High-efficiency organic polymer light-emitting heterostructure devices on flexible plastic substrates. *Appl Phys Lett* 2000; 76: 661-663.
- [53] Wager JF. *Transparent electronics*. Science 2003; 300: 1245-1246.
- [54] Garnich F, Yu PC, Lampert CM. Hydrated manganese oxide as a counter-electrode material for an electrochromic optical switching device. *Solar Energy Materials* 1990; 20: 265-275.
- [55] Grivas C, Mallis S, Boutsikaris L, Gill DS, Vainos NA, Chandler PJ. Growth and performance of pulsed laser deposited indium oxide thin-film holographic recorders. *Laser Phys* 1998; 8: 326-330.
- [56] Moschovis K, Gagaoudakis E, Chatzitheodoridis E, *et al.* Study of the ambient optical recording dynamics on sputtered indium oxide thin films. *Appl Phys A* 1998; 66: 651-654.
- [57] Moller S, Perlov C, Jackson W, Taussig C, Forest SR, A. polymer/semiconductor write-once read-many-times memory. *Nature* 2003; 426: 166-168.
- [58] Hayes RA, Feenstra BJ. Video-speed electronic paper based on electrowetting. *Nature* 2003; 425: 383-385.
- [59] Cornia RL, Fenn JB, Memarian H, Ringer R. Proc. 41st Annual Technical Conference, Soc. of Vacuum Coaters, Boston 1998; p. 452.
- [60] Cairns DR, Witte RP, Sparacin DK, *et al.* Strain-dependent electrical resistance of tin-doped indium oxide on polymer substrates. *Appl Phys Lett* 2000; 76: 1425-1427.
- [61] Banerjee AN, Ghosh CK, Chattopadhyay KK, *et al.* Low-temperature deposition of ZnO thin films on PET and glass substrates by DC-sputtering technique. *Thin Solid Films* 2006; 496: 112-116.
- [62] Seager, CH, McIntyre DC, Warren WL, Tuttle BA. Charge trapping and device behavior in ferroelectric memories. *Appl Phys Lett* 1996; 68: 2660-2662.
- [63] Prince MWJ, Gross-Holtz KO, Muller G, *et al.* A ferroelectric transparent thin-film transistor. *Appl Phys Lett* 1996; 68: 3650-3652.
- [64] Sato H, Minami T, Takata S, Yamada T. Transparent conducting p-type NiO thin films prepared by magnetron sputtering. *Thin Solid Films* 1993; 236: 27-31.
- [65] Kawazoe H, Yasukawa M, Hyodo H, Kurita M, Yanagi H, Hosono H. P-type electrical conduction in transparent thin films of CuAlO₂. *Nature* 1997; 389: 939-942.
- [66] Ueda K, Hase T, Yanagi H, *et al.* Epitaxial growth of transparent p-type conducting CuGaO₂ thin films on sapphire (001) substrates by pulsed laser deposition. *J Appl Phys* 2001; 89: 1790-1793.
- [67] Yanagi H, Hase T, Ibuki S, Ueda K, Hosono H. Bipolarity in electrical conduction of transparent oxide semiconductor CuInO₂ with delafossite structure. *Appl Phys Lett* 2001; 78: 1583-1585.
- [68] Yanagi H, Ueda K, Ohta H, Orita M, Hirano M, Hosono H. Fabrication of all oxide transparent p-n homojunction using bipolar CuInO₂ semiconducting oxide with delafossite structure. *Solid State Comm* 2001; 121: 15-17.

- [69] Tate J, Jayaraj MK, Draeseke AD, *et al.* p-Type oxides for use in transparent diodes. *Thin Solid Films* 2002; 411: 119-124.
- [70] Duan N, Sleight AW, Jayaraj MK, Tate J. Transparent p-type conducting CuScO_{2+x} films. *Appl Phys Lett* 2000; 77: 1325-1326.
- [71] Nagrajan R, Draeseke AD, Sleight AW, Tate J. p-type conductivity in $\text{CuCr}_{1-x}\text{Mg}_x\text{O}_2$ films and powders. *J Appl Phys* 2001; 89: 8022-8025.
- [72] Jayaraj MK, Draeseke AD, Tate J, Sleight AW. p-Type transparent thin films of $\text{CuY}_{1-x}\text{Ca}_x\text{O}_2$. *Thin Solid Films* 2001; 397: 244-248.
- [73] Nagrajan R, Duan N, Jayaraj MK, *et al.* p-Type conductivity in the delafossite structure. *Int. J Inorg Mater* 2001; 3: 265-270.
- [74] Nagrajan R, Uma S, Jayaraj MK, Tate J, Sleight AW. *Solid State Science. Solid State Science* 2002; 4: 787-792.
- [75] Kandpal HC, Seshadri R. First-principles electronic structure of the delafossites ABO_2 (A=Cu, Ag, Au; B=Al, Ga, Sc, In, Y): evolution of d^{10} - d^{10} interactions. *Solid State Sciences* 2002; 4: 1045-1052.
- [76] Kudo A, Yanagi H, Hosono H, Kawazoe H. SrCu_2O_2 : A p-type conductive oxide with wide band gap. *Appl Phys Lett* 1998; 73: 220-222.
- [77] Windisch Jr. CF, Ferris KM, Exarhos GJ. Synthesis and characterization of transparent conducting oxide cobalt-nickel spinel films. *J Vac Sci Technol A* 2001; 19: 1647-1651.
- [78] Windisch Jr. CF, Engelhard MH, Stewart DC. Infrared transparent spinel films with p-type conductivity. *Thin Solid Films* 2001; 398-399: 45.
- [79] Hiramatsu H, Ueda K, Ohta H, Orita M, Hirano M, Hosono H. Preparation of transparent p-type $(\text{La}_{1-x}\text{Sr}_x\text{O})\text{CuS}$ thin films by r.f. sputtering technique. *Thin Solid Films* 2002; 411: 125-128.
- [80] Ueda K, Inoue S, Hirose S, Kawazoe H, Hosono H. Transparent p-type semiconductor: LaCuOS layered oxysulfide. *Appl Phys Lett* 2000; 77: 2701-2703.
- [81] Ueda K, Inoue S, Hosono H, Sarukura N, Hirano M. Room-temperature excitons in wide-gap layered-oxysulfide semiconductor: LaCuOS . *Appl Phys Lett* 2001; 78: 2333-2335.
- [82] Ueda K, Hosono H. Band gap engineering, band edge emission, and p-type conductivity in wide-gap $\text{LaCuOS}_{1-x}\text{Se}_x$ oxychalcogenides. *J Appl Phys* 2002; 91: 4768-4770.
- [83] Takase K, Koyano M, Shimizu T, *et al.* Electrical resistivity and photoluminescence spectrum of layered oxysulfide $(\text{LaO})\text{CuS}$. *Solid State Comm* 2002; 123: 531-534.
- [84] Hiramatsu H, Orita M, Hirano M, Ueda K, Hosono H. Electrical conductivity control in transparent p-type $(\text{LaO})\text{CuS}$ thin films prepared by rf sputtering. *J Appl Phys* 2002; 91: 9177-9181.
- [85] Hiramatsu H, Ueda K, Takafuji K, *et al.* Intrinsic excitonic photoluminescence and band-gap engineering of wide-gap p-type oxychalcogenide epitaxial films of LnCuOCh (Ln = La, Pr, and Nd; Ch = S or Se) semiconductor alloys. *J Appl Phys* 2003; 94: 5805-5808.
- [86] Hiramatsu H, Ueda K, Ohta H, Hirano M, Kamiya T, Hosono H. Degenerate p-type conductivity in wide-gap $\text{LaCuOS}_{1-x}\text{Se}_x$ ($x = 0-1$) epitaxial films. *Appl Phys Lett* 2003; 82: 1048-1050.
- [87] Ueda K, Hiramatsu H, Ohta H, Hirano M, Kamiya T, Hosono H. Single-atomic-layered quantum wells built in wide-gap semiconductors LnCuOCh (Ln = lanthanide, Ch = chalcogen). *Phys Rev B* 2004; 69: 155305.
- [88] Zhu WJ, Huang YZ, Dong C, Zhao ZX. Synthesis and crystal structure of new rare-earth copper oxyselenides: RCuSeO (R=La, Sm, Gd and Y). *Mater Res Bull* 1994; 29: 143-147.
- [89] Palazzi M, Carcaly C, Flahaut J. Un nouveau conducteur ionique $(\text{LaO})\text{AgS}$. *J Solid State Chem* 1980; 35: 150-155.
- [90] Minami T, Shimokawa K, Miyata T. p-type transparent conducting In_2O_3 - Ag_2O thin films prepared by rf magnetron sputtering. *J Vac Sci Technol A* 1998; 16: 1218-1221.
- [91] Lander JJ. Reactions of lithium as a donor and an acceptor in ZnO. *J Phys Chem Solids* 1960; 15: 324-334.
- [92] Hümmer K. Interband magnetoreflection of ZnO. *Phys Stat Solidi B* 1973; 56: 249-260.
- [93] Sato Y, Sato S. Preparation and some properties of nitrogen-mixed ZnO thin films. *Thin Solid Films* 1996; 281-282: 445-448.
- [94] Minegishi K, Koiwai Y, Kikuchi Y, Yano K, Kasuga M, Shimizu A. Growth of p-type Zinc oxide films by chemical vapor deposition. *Jpn. J Appl Phys* 1997; 36: L1453-L1455.
- [95] Guo XL, Tabata H, Kawai T. Epitaxial growth and optoelectronic properties of nitrogen-doped ZnO films on $(1120) \text{Al}_2\text{O}_3$ substrate. *J. Cryst. Growth*, 2001; 237-239: 544-547.
- [96] Wang J, Du G, Zhao B, *et al.* Epitaxial growth of NH_3 -doped ZnO thin films on (0224) oriented sapphire substrates. *J Cryst Growth* 2003; 255: 293-297.
- [97] Look DC, Reynolds DC, Litton CW, Jones RL, Eason DB, Cantwell G. Characterization of homoepitaxial p-type ZnO grown by molecular beam epitaxy. *Appl Phys Lett* 2002; 81: 1830-1832.
- [98] Ashrafi ABMA, Suemune I, Kumano H, Tanaka S. Nitrogen-Doped p-Type ZnO Layers Prepared with H_2O Vapor-Assisted Metalorganic Molecular-Beam Epitaxy. *Jpn. J Appl Phys* 2002; 41: L1281-L1284.
- [99] Ryu YR, Zhu S, Look DC, Wrobel JM, Joeng HM, White HW. Synthesis of p-type ZnO films. *J. Cryst. Growth* 2000; 216: 330-334.
- [100] Yamamoto T, Yoshida HK. Solution using a codoping method to *Unipolarity* for the fabrication of p-Type ZnO. *Jpn J Appl Phys* 1999; 38: L166-L169.
- [101] Joseph M, Tabata H, Kawai T. P-Type electrical conduction in ZnO thin films by Ga and N codoping. *Jpn J Appl Phys* 1999; 38: L1205-L1207.
- [102] Yanagi H, Inoue S, Ueda K, Kawazoe H, Hosono H, Hamada N. Electronic structure and optoelectronic properties of transparent p-type conducting CuAlO_2 . *J Appl Phys* 2000; 88: 4159-4163.
- [103] Kawazoe H, Yanagi H, Ueda K, Hosono H. Transparent p-Type conducting oxides: design and fabrication of p-n heterojunctions. *MRS Bull* 2000; pp. 28.
- [104] Stauber RE, Perkins JD, Parilla PA, Ginley DS. Thin film growth of transparent p-type CuAlO_2 . *Electrochem Solid State Lett* 1999; 2: 654-656.
- [105] Kakehi Y, Nakao S, Satoh K, Yotsuya T. Properties of copper-scandium oxide thin films prepared by pulsed laser deposition. *Thin Solid Films* 2003; 445: 294-298.
- [106] Banerjee AN, Kundoo S, Chattopadhyay KK. Synthesis and characterization of p-type transparent conducting CuAlO_2 thin film by DC sputtering. *Thin Solid Films* 2003; 440: 5-10.
- [107] Banerjee AN, Maity R, Ghosh PK, Chattopadhyay KK. Thermoelectric properties and electrical characteristics of sputter-deposited p- CuAlO_2 thin films. *Thin Solid Films* 2005; 474: 261-266.
- [108] Banerjee AN, Chattopadhyay KK. Low-threshold field emission from transparent p-type conducting CuAlO_2 thin film prepared by dc sputtering. *Appl Surf Sci* 2004; 225: 243-249.
- [109] Banerjee AN, Ghosh CK, Chattopadhyay KK. Effect of excess oxygen on the electrical properties of transparent p-type conducting CuAlO_{2+x} thin films. *Sol. Energy Mater Sol Cells* 2005; 89: 75-83.
- [110] Banerjee AN, Chattopadhyay KK. P-Type transparent semiconducting delafossite CuAlO_{2+x} thin film: promising material for optoelectronic devices and field-emission displays. in materials science research trends. Ed Olivante MB Nova Science Publishers NY, USA (in press).
- [111] Banerjee AN, Chattopadhyay KK. Recent Developments in the emerging field of crystalline P-Type transparent conducting oxide thin films. *Progress in Crystal Growth and Characterization of Materials* 2005; 50: 52-105.
- [112] Ong CH, Gong H. Effects of aluminum on the properties of p-type Cu-Al-O transparent oxide semiconductor prepared by reactive co-sputtering. *Thin Solid Films* 2003; 445: 299-303.
- [113] Tsuboi N, Takahashi Y, Kobayashi S, Shimizu H, Kato K, Kaneko F. Delafossite CuAlO_2 films prepared by reactive sputtering using Cu and Al targets. *J Phys Chem Solids* 2003; 64: 1671-1674.
- [114] Banerjee AN, Maity R, Chattopadhyay KK. Preparation of p-type transparent conducting CuAlO_2 thin films by reactive DC sputtering. *Materials Letters* 2003; 58: 10-13.
- [115] Banerjee AN, Ghosh CK, Das S, Chattopadhyay KK. Electro-optical characteristics and field-emission properties of reactive DC-sputtered p- CuAlO_{2+x} thin films. *Physica B* 2005; 370: 264-276.
- [116] Banerjee AN, Chattopadhyay KK. Reactive-Sputtered Wide-Bandgap p-Type semiconducting spinel AB_2O_4 and delafossite ABO_2 thin films for 'transparent electronics', in reactive rputter deposition. Eds Mahieu S Depla D Springer NY, USA (accepted for publication).
- [117] Reddy AS, Reddy PS, Uthanna S, Rao GM. Characterization of CuAlO_2 films prepared by dc reactive magnetron sputtering. *J Mater Sci Mater Electron* 2006; 17: 615-620.

- [118] Wang Y, Gong H. High-Conductivity p-type transparent copper aluminum oxide film prepared by plasma-enhanced MOCVD. *Chemical vapor deposition* 2000; 6: 285-288.
- [119] Gong H, Wang Y, Luo Y. Nanocrystalline p-type transparent Cu-Al-O semiconductor prepared by chemical-vapor deposition with Cu(acac)₂ and Al(acac)₃ precursors. *Appl Phys Lett* 2000; 76: 3959-3961.
- [120] Wang Y, Gong H, Zhu F, Liu L, Huang L, Huan ACH. Optical and electrical properties of p-type transparent conducting Cu-Al-O thin films prepared by plasma enhanced chemical vapor deposition. *Materials Science and Engineering B* 2001; 85: 131-134.
- [121] Ohta H, Nomura K, Orita M, *et al.* Single-crystalline films of the homologous series in GaO₃(ZnO)_m Grown by reactive solid-phase epitaxy. *Adv Funct Mater* 2003; 13: 139-144.
- [122] Ohta H, Nomura K, Orita M, *et al.* Novel film growth technique of single crystalline In₂O₃(ZnO)_m (m=integer) homologous compound. *Thin Solid Films* 2002; 411: 147151.
- [123] Hiramatsu H, Ueda K, Ohta H, Orita M, Hirano M, Hosono H. Heteroepitaxial growth of a wide-gap p-type semiconductor, LaCuOS. *Appl Phys Lett* 2002; 81: 598-600.
- [124] Bobeico E, Varsano F, Minarini C, F. Roca, P-type strontium-copper mixed oxide deposited by e-beam evaporation. *Thin Solid Films* 2003; 444: 70-74.
- [125] Kim DS, Choi SY. Wet-oxidation effect on p-type transparent conducting CuAlO₂ thin film. *Phys Stat Solidi A* 2005, 202: R167-R169.
- [126] Shy JH, Tseng BH. Characterization of CuAlO₂ thin film prepared by rapid thermal annealing of an Al₂O₃/Cu₂O/sapphire structure. *J Phys. Chem. Solids* 2005; 66: 2123-2126.
- [127] Tonooka K, Shimokawa K, Nishimura O. Properties of copper-aluminum oxide films prepared by solution methods. *Thin Solid Films* 2002; 411: 129-133.
- [128] Ohashi M, Iida Y, Morikawa H. Preparation of CuAlO₂ Films by Wet Chemical Synthesis. *J Am Ceram Soc* 2002; 85: 270-272.
- [129] Shahriari DY, Barnabè A, Mason TO, Poepelmeier KR. A high-yield hydrothermal preparation of CuAlO₂. *Inorg Chem* 2001; 40: 5734-5735.
- [130] Gao S, Zhao Y, Gou P, Chen N, Xie Y. Preparation of CuAlO₂ nanocrystalline transparent thin films with high conductivity. *Nanotechnology* 2003; 14: 538-541.
- [131] Bouzidi C, Bouzouita H, Timoumi A, Rezig B. Fabrication and characterization of CuAlO₂ transparent thin films prepared by spray technique. *Mater Sci Engg B* 2005; 118: 259-263.
- [132] Park S, Keszlör DA, Valencia MM, Hoffman RL, Bender JP, Wager JF. Transparent p-type conducting BaCu₂S₂ films. *Appl Phys Lett* 2002; 80: 4393-4394.
- [133] Wu WJ, Huang YZ, Wu F, Dong C, Chen H, Zhao ZX. Synthesis and crystal structure of barium copper fluochalcogenides:[BaCuFQ (Q=S,Se)]. *Mater Res Bull* 1994; 29: 505-508.
- [134] Yanagi H, Park S, Draeseke AD, Keszlör DA, Tate J. P-type conductivity in transparent oxides and sulfide fluorides. *J Solid State Chem* 2003; 175: 34-38.
- [135] Thomas G. Materials science: Invisible circuits. *Nature* 1997; 389: 907-908.
- [136] Kudo A, Yanagi H, Ueda K, Hosono H, Kawazoe H, Yano Y. Fabrication of transparent p-n heterojunction thin film diodes based entirely on oxide semiconductors. *Appl Phys Lett* 1999; 75: 2851-2853.
- [137] Ohta H, Kawamura K, Orita M, Sarukura N, Hirano M, Hosono H. Characterisation of reactively sputtered silicon oxide for thin-film transistor fabrication. *Electron Lett* 2000; 36: 984-985.
- [138] Ohta H, Kawamura K, Orita M, Hirano M, Sarukura N, Hosono H. Current injection emission from a transparent p-n junction composed of p-SrCu₂O₂/n-ZnO. *Appl Phys Lett* 2000; 77: 475-547.
- [139] Ohta H, Orita M, Hirano M. Fabrication and characterization of ultraviolet-emitting diodes composed of transparent p-n heterojunction, p-SrCu₂O₂ and n-ZnO. *J Appl Phys* 2001; 89: 5720-5725.
- [140] Hosono H, Ohta H, Hayashi K, Orita M, Hirano M. Near-UV emitting diodes based on a transparent p-n junction composed of heteroepitaxially grown p-SrCu₂O₂ and n-ZnO. *J Cryst Growth* 2002; 237-239: 496-502.
- [141] Hoffman RL, Wager JF, Jayaraj MK, Tate J. Electrical characterization of transparent p-i-n heterojunction diode. *J Appl Phys* 2001; 90: 5763-5767.
- [142] Jayaraj MK, Draeseke AD, Tate J, Hoffman RL, Wager JF. Transparent heterojunction thin film diode. *Mat Res Soc Proc* 2001; 666: F4.1-F4.5.
- [143] Tonooka K, Bando H, Aiura Y. Photovoltaic effect observed in transparent p-n heterojunctions based on oxide semiconductors. *Thin Solid Films* 2003; 445: 327-334.
- [144] Banerjee AN, Nandy S, Ghosh CK, Chattopadhyay KK. Fabrication and characterization of all-oxide heterojunction p-CuAlO_{2-x}/n-Zn_{1-x}Al_xO transparent diode for potential application in "invisible electronics". *Thin Solid Films* 2007; 515: 7324-7330.
- [145] Banerjee AN, Chattopadhyay KK. Electro-optical properties of all-oxide p-CuAlO₂ / n-ZnO: All transparent heterojunction thin film diode fabricated on glass substrate. *Central European J Phys* (in press).
- [146] Hwang DK, Bang KH, Jeong MC, Myoung JM. Effects of RF power variation on properties of ZnO thin films and electrical properties of p-n homojunction. *J Cryst Growth* 2003; 254: 449-455.
- [147] Tüzemen S, Xiong G, Wilkinson J, Mischuck B, Ucer KB, Williams RT. Production and properties of p-n junctions in reactively sputtered ZnO. *Physica B* 2003; 308-310: 1197-1200.
- [148] Aoki T, Hatanaka Y, Look DC. ZnO diode fabricated by excimer-laser doping. *Appl Phys Lett* 2000; 76: 3257-3258.
- [149] Prins MWJ, Grosse-Holz KO, Müller G. *et al.* A ferroelectric transparent thin-film transistor. *Appl Phys Lett* 1996; 68: 3650-3652.
- [150] Prins MWJ, Zinnemers SE, Cillessen JFM, Giesbers JB. Depletion layer thin film transistors with a ferroelectric insulator. *Appl Phys Lett* 1997; 70: 458-460.
- [151] Hoffman RL, Norris BJ, Wager JF. ZnO-based transparent thin film transistors. *Appl Phys Lett* 2003; 82: 733-735.
- [152] Masuda S, Kitamura K, Okumura Y, Miyatake S, Tabata H, Kawai T. Transparent thin film transistors using ZnO as an active channel layer and their electrical properties. *J Appl Phys* 2003; 93: 1624-1630.
- [153] Garcia PF, McLean RS, Reilly MH, Nunes G Jr.. Transparent ZnO thin-film transistor fabricated by rf magnetron sputtering. *Appl Phys Lett* 2003; 82: 1117-1119.
- [154] Nomura K, Ohta H, Ueda K, Kamiya T, Hirano M, Hosono H. Thin-film transistor fabricated in single-crystalline transparent oxide semiconductor. *Science* 2003; 300: 1269-1272.
- [155] Ohta H, Nomura K, Hiramatsu H, *et al.* Frontier of transparent oxide semiconductors. *Solid-State Electronics* 2003; 47: 2261-2267.
- [156] Efros AL, Efros AL. Absorption of light in a semiconductor sphere. *Sov Phys Semicond* 1982; 16: 772-775.
- [157] Brus LE. Electron-electron and electron-hole interactions in small semiconductor crystallites: The size dependence of the lowest excited electronic state. *J Chem Phys* 1984; 80: 4403-4409.
- [158] Cox AJ, Louderback JG, Bloomfield LA. Experimental observation of magnetism in rhodium clusters. *Phys Rev Lett* 1993; 71: 923-926.
- [159] Alivisatos AP. Semiconductor Clusters, Nanocrystals and Quantum Dots. *Science* 1996; 271: 933-937.
- [160] Heath JR. The chemistry of size and order on a nanometer scale. *Science* 1995; 270: 1315-1316.
- [161] Lorke A, Kotthaus JP. Coupling of quantum dots on GaAs. *Phys Rev Lett* 1990; 64: 2559-2562.
- [162] Li Q, Wang C. Fabrication of wurtzite ZnS nanobelts via simple thermal evaporation. *Appl Phys Lett* 2003; 83: 359-361.
- [163] Demel T, Heitmann D, Grambow P, Ploog K. One-dimensional plasmons in AlGaAs/GaAs quantum wires. *Phys Rev Lett* 1991; 66: 2657-2662.
- [164] Klein DL, Roth R, Lim AKL, Alivisatos AP, McEuen PL. A single-electron transistor made from a cadmium selenide nanocrystal. *Nature* 1997; 389: 699-700.
- [165] Feldheim DL, Keating CD. Self-assembly of single electron transistors and related devices. *Chem Soc Rev* 1998; 27: 1-12.
- [166] DeVault D. A method of teaching the electronic structure of the atom. *J Chem Educ* 1944; 21: 526-534.
- [167] Bailar JC Jr., Emelús HJ, Sir Ronald N, Trotman-Dickenson AF. *Comprehensive inorganic chemistry*; Pergamon: New York, NY, 1973.
- [168] Leung YK, Khan AK, Kos JF, Koffyberg FP. *Proc. Nat. Conf. Solar Energy*; Solar Energy Society of Canada Montreal 1981; pp. 124.
- [169] Dahl JP, Switendick AC. Energy bands in cuprous oxide. *J. Phys. Chem Solids* 1966; 27: 931-942.

- [170] Hayashi M, Katsuki K. Absorption spectrum of cuprous oxide. *J Phys Soc Jpn* 1950; 5: 380B-381.
- [171] Shannon RD, Rogers DB, Prewitt CT. Chemistry of noble metal oxides. I. Syntheses and properties of ABO_2 delafossite compounds. *Inorg Chem* 1971; 10: 713-718.
- [172] Prewitt CT, Shannon RD, Rogers DB. Chemistry of noble metal oxides. II. Crystal structures of platinum cobalt dioxide, palladium cobalt dioxide, copper iron dioxide, and silver iron dioxide. *Inorg Chem* 1971; 10: 719-723.
- [173] Rogers DB, Shannon RD, Prewitt CT, Gilson JL. Chemistry of noble metal oxides. III. Electrical transport properties and crystal chemistry of ABO_2 compounds with the delafossite structure. *Inorg Chem* 1971; 10: 723-727.
- [174] Otabe T, Ueda K, Kudoh A, Hosono H, Kawazoe H. n-type electrical conduction in transparent thin films of delafossite-type $AgInO_2$. *Appl Phys Lett* 1998; 72: 1036-1038.
- [175] Kofstad P. Nonstoichiometry, diffusion, and electrical conductivity in binary metal oxides; Wiley-Interscience 1972; pp.19.
- [176] Koumoto K, Koduka H, Seo WS. Thermoelectric properties of single crystal $CuAlO_2$ with a layered structure. *J Mater Chem* 2001; 11: 251-253.
- [177] Cava RJ, Peck WF Jr., Krajewski JJ, Cheong SW, Hwang HY. Electrochemical and high pressure superoxygenation of $YCuO_{2-x}$ and $LaCuO_{2-x}$ delafossites. *J Mater Res* 1994; 9: 314-317.
- [178] Cava RJ, Zandbergen HW, Ramirez AP, et al. $LaCuO_{2.5+x}$ and $YCuO_{2.5+x}$ Delafossites: Materials with Triangular Cu^{2+6} Planes. *J Solid State Chem* 1993; 104: 437-452.
- [179] Jayaraj MK, Draeseke A, Tate J, Duan N, Sleight AW. Proceedings of the MRS Workshop on Transparent Conductive Oxide, Denever, CO 19-20 June, 2000.
- [180] Lalić MV, Filho JM, Carbonari AW, Saxena RN, Moralles M. Influence of Cd impurity on the electronic properties of $CuAlO_2$ delafossite: first-principles calculations. *J Phys Condens Matter* 2002; 14: 5517-5528.
- [181] Lalić MV, Filho JM, Carbonari AW, Saxena RN. Changes induced by the presence of Zn or Ni impurity at Cu sites in $CuAlO_2$ delafossite. *Solid State Comm* 2003; 125: 175-178.
- [182] Benko FA, Koffyberg FP. Opto-electronic properties of p- and n-type delafossite, $CuFeO_2$. *J Phys Chem Solids* 1987; 48: 431-434.
- [183] Cava RJ, Peck WF Jr., Krajewski JJ, Cheong SW, Hwang HY. Electrochemical and high pressure superoxygenation of $YCuO_{2-x}$ and $LaCuO_{2-x}$ delafossites. *J Mater Res* 1994; 9: 314-317.
- [184] Shahriari, D.Y., Barnabé, A, Mason, T.O., Poeppelmeier, K.R.: US20056979435 (2005).
- [185] Benko FA, Coffyberg FP. Opto-electronic properties of $CuAlO_2$. *J Phys Chem Solids* 1984; 45: 57-59.
- [186] Lee C, Lim J. Effects of the annealing temperature on the electrical properties of p-Type ZnO films grown on (0001) sapphire substrates by using atomic layer epitaxy. *Journal of the Korean Physical Society* 2006; 49: 913-917.
- [187] Bian JM, Li XM, Zhang CY, Yu WD, Gao XD. p-type ZnO films by monodoping of nitrogen and ZnO-based p-n homojunctions. *Applied Physics Letters* 2004; 85: 4070-4072.
- [188] Tsukazaki A, Ohtomo A, Onuma T, et al. Repeated temperature modulation epitaxy for p-type doping and light-emitting diode based on ZnO. *Nature Materials* 2005; 4: 42-46.
- [189] Yan Y, Zhang SB, Pantelides ST. Control of doping by impurity chemical potentials: Predictions for p-Type ZnO. *Phys Rev Lett* 2001; 86: 5723-5726.
- [190] Liang HW, Lu YM, Shen DZ, Liu YC, Yan JF, Shan CX, Li BH, Zhang ZZ, Zhang JY, Fan XW. P-type ZnO thin films prepared by plasma molecular beam epitaxy using radical NO. *phys. stat. sol. (a)*, 2005; 202: 1060-1065
- [191] Zeng YJ, Ye ZZ, Lu YF, et al. Investigation on ultraviolet photoconductivity in p-type ZnO thin films. *Chemical Physics Letters* 2007; 441: 115-118.
- [192] Aoki T, Shimizu Y, Miyake A, Nakamura A, Nakanishi Y, Hatanaka Y. p-Type ZnO Layer Formation by Excimer Laser Doping. *phys stat sol B* 2002; 229: 911-914.
- [193] Kim KK, Kim HS, Hwang DK, Lim JH, Park SJ. Realization of p-type ZnO thin films via phosphorus doping and thermal activation of the dopant. *Appl Phys Lett* 2003; 83: 63-65.
- [194] Kasuga M, Ogawa S. Electronic properties of vapor-grown heteroepitaxial ZnO film on sapphire. *Jpn J Appl Phys* 1983; 22: 794-794.
- [195] Park CH, Zhang SB, Wei SH. Origin of p-type doping difficulty in ZnO: The impurity perspective. *Phys Rev B* 2002; 66: 073202-1 - 073202-1.
- [196] Yan Y, Zhang SB, Pantelides ST. Control of doping by impurity chemical potentials: Predictions for p-Type ZnO. *Phys Rev Lett* 2001; 86: 5723-5726.
- [197] Tamura K, Makino T, Tsukazaki A, et al. Donor-acceptor pair luminescence in nitrogen-doped ZnO films grown on lattice-matched $ScAlMgO_4$ (0001) substrates. *Solid State Comm* 2003; 127: 265-269.
- [198] Nakahara K, Takasu H, Fons P, et al. Interactions between gallium and nitrogen dopants in ZnO films grown by radical-source molecular-beam epitaxy. *Appl Phys Lett* 2001; 79: 4139-4141.
- [199] Tsukazaki A, Saito H, Tamura K, et al. Systematic examination of carrier polarity in composition spread ZnO thin films codoped with Ga and N. *Appl Phys Lett* 2002; 81: 235-237.
- [200] Yang LL, Ye ZZ, Zhu LP, Zeng YJ, Lu YF, Zhao BH. Fabrication of p-Type ZnO thin films via DC reactive magnetron sputtering by using Na as the dopant source. *Journal of Electronic Materials* 2007; 36: 498-501.
- [201] Dietl T, Ohno H, Matsukura F, Cibert J, Ferrand D. Zener Model Description of ferromagnetism in zinc-blende magnetic semiconductors. *Science* 2000; 287: 1019-1022.
- [202] Tan ST, Chen BJ, Sun XW, Yu MB, Zhang XH, Chua SJ. Realization of intrinsic p-type ZnO thin films by metal organic chemical vapor deposition. *Journal of Electronic Materials* 2005; 34: 1172-1176.
- [203] Triboulet R, Perrière J. Epitaxial growth of ZnO films. *Progress in Crystal Growth and Characterization of Materials* 2003; 65-138.
- [204] Dai LP, Deng H, Mao FY, Zang JD. The recent advances of research on p-type ZnO thin film. *J Mater Sci Mater Electron* (DOI 10.1007/s10854-007-9398-y).
- [205] Yan, Y., Zhang, S.: US20056908782 (2005).
- [206] Hiroshi, Y., Tetsuya, Y.: US20036527858 (2003).
- [207] Kakuya, I., Paul, F., Koji, M., Akimasa, Y., Shigeru, N., Ken, N.: US20036638846 (2003).
- [208] White, H.W., Zhu, S., Ryu Y.: US20067033435 (2006).
- [209] Banerjee AN, Chattopadhyay KK. Size-dependent optical properties of sputter-deposited nanocrystalline P-type transparent $CuAlO_2$ thin films *J Appl Phys* 2005; 97: 084308-1 - 084308-1.
- [210] Jacob A, Parent C, Boutinaud P, et al. Luminescent properties of delafossite-type oxides $LaCuO_2$ and $YCuO_2$. *Solid State Comm* 1997; 103: 529-532.
- [211] Xiang B, Wang P, Zhang X, et al. Rational synthesis of p-Type zinc oxide nanowire arrays using simple chemical vapor deposition. *Nano Lett* 2007; 7: 323-328.
- [212] Hirsch P, Howie A, Nicholson RB, Pashley DW, Whelan MJ. *Electron microscopy in thin crystals*; Robert E. Krieger Publishing Co.: Huntington, NY, 1977.
- [213] Powder Diffraction File; Joint Committee on Powder Diffraction Standards, ASTM; Philadelphia, PA, 1967; Card # 35-1401.
- [214] Willardson, RK, Beer AC. *Semiconductors and Semimetals*; Vol. 8, Academic Press: New York and London, 1971.
- [215] Yoshida HK, Koyanagi T, Funashima H, Harima H, Yanase A. Engineering of nested Fermi surface and transparent conducting p-type Delafossite $CuAlO_2$: possible lattice instability or transparent superconductivity?. *Solid State Comm* 2003; 126: 135-139.
- [216] Koyanagi T, Harima H, Yanase A, Yoshida HK. Materials design of p-type transparent conducting oxides of delafossite $CuAlO_2$ by super-cell FLAPW method. *J Phys Chem Solids* 2003; 64: 1443-1446.
- [217] Lalić MV, Filho MJ. Correlation between the EFG values measured at the Cd impurity in a group of Cu-based delafossites and the semiconducting properties of the latter. *Hyperfine Interactions* 2004 ; 158 : 89-93.
- [218] Mizoguchi H, Hirano M, Fujitsu S, Takeuchi T, Ueda K, Hosono H. $ZnRh_2O_4$: A p-type semiconducting oxide with a valence band composed of a low spin state of Rh^{3+} in a $4d^6$ configuration. *Appl Phys Lett* 2002 ; 80 : 1207-1209.
- [219] Dekkers M, Rijnders G, Blank DHA. $ZnIr_2O_4$, a p-type transparent oxide semiconductor in the class of spinel zinc- d^6 -transition metal oxide. *Appl Phys Lett* 2007 ; 90 : 021903-1 - 021903-3.
- [220] Ji Z, He Z, Song Y, Liu K, Ye Z. Fabrication and characterization of indium-doped p-type SnO_2 thin films. *J Cryst Growth* 2003 ; 259: 282-285.

- [221] Huang Y, Ji Z, Chen C. Preparation and characterization of p-type transparent conducting tin-gallium oxide films. *Appl Surf Sci* 2007; 253: 4819-4822.
- [222] Tonooka K, Kikuchi N. Preparation of transparent CuCrO₂/Mg/ZnO p-n junctions by pulsed laser deposition. *Thin Solid Films* 2006; 515: 2415-2418.
- [223] Banerjee AN, Chattopadhyay KK. Electro-optical properties of all-oxide p-CuAlO₂/n-ZnO: Al transparent heterojunction thin film diode fabricated on glass substrate. *Central european J Phys* (in press).
- [224] Park K, Ko KY, Seo WS. Effect of partial substitution of Ca for Al on the microstructure and high-temperature thermoelectric properties of CuAlO₂. *Mater Sci Engg B* 2006; 129: 1-7.
- [225] Hicks LD, Dresselhaus MS. Effect of quantum-well structures on the thermoelectric figure of merit. *Phys Rev B* 1993; 47: 12727-12731.
- [226] Hicks LD, Herman TC, Dresselhaus MS. Use of quantum-well superlattices to obtain a high figure of merit from nonconventional thermoelectric materials. *Appl Phys Lett* 1993; 63: 3230-3232.
- [227] Hicks LD, Dresselhaus MS. Thermoelectric figure of merit of a one-dimensional conductor *Phys Rev B* 47 (1993) 16631-16634.
- [228] Goldsmith JH. *Thermoelectric Refrigeration*, Plenum, New York, 1964.
- [229] Banerjee AN, Ghosh CK, Das S, Chattopadhyay KK. Electro-optical characteristics and field-emission properties of reactive D. C. Sputtered p-CuAlO_{2+x} Thin Films. *Physica B* 2005; 370: 264-276.
- [230] Banerjee AN, Chattopadhyay KK. Low-threshold field-emission from transparent P-Type conducting CuAlO₂ thin film prepared by D. C. sputtering. *Appl Surf Sci* 2004; 225: 243-249.
- [231] Zheng XG, Taniguchi K, Takahashi A, Liu Y, Xu CN. Room temperature sensing of ozone by transparent p-type semiconductor CuAlO₂. *Appl Phys Lett* 2004; 85: 1728-1729.
- [232] Sauter D, Weimar U, Noetzel G, Mitrovics J, Gopel W. Development of modular ozone sensor system for application in practical use. *Sens Actuators B* 2000; 69: 1-9.
- [233] Kim SR, Hong HK, Kwon CH, Yun DH, Lee K, Sung YK. Ozone sensing properties of In₂O₃-based semiconductor thick films. *Sens Actuators B* 2000; 66: 59-62.
- [234] Gagaoudakis E, Bender M, Douloufakis E, *et al.* The influence of deposition parameters on room temperature ozone sensing properties of InO_x films. *Sens Actuators B* 2001; 80: 155-161.
- [235] Bender M, Gagaoudakis E, Douloufakis E, *et al.* Production and characterization of zinc oxide thin films for room temperature ozone sensing. *Thin Solid Films* 2002; 418: 45-50.
- [236] Koriche N, Bouguelia A, Aider A, Trari M. Photocatalytic hydrogen evolution over delafossite CuAlO₂. *International Journal of Hydrogen Energy* 2005; 30: 693-699.
- [237] Kizaki H, Sato K, Yanase A, Katayama-Yoshida H. Ab initio calculations of CuAlO₂-based dilute magnetic semiconductor. *Physica B* 2006; 376-377: 812-815.

Not For Distribution